Available online at www.sciencedirect.com

ScienceDirect

Geochimica et Cosmochimica Acta 207 (2017) 256–276

Geochimica et Cosmochimica Acta

www.elsevier.com/locate/gca

Iron oxide reduction in methane-rich deep Baltic Sea sediments

Matthias Egger [a,*], Mathilde Hagens [a], Célia J. Sapart [b,c], Nikki Dijkstra [a], Niels A.G.M. van Helmond [a], José M. Mogollón [a], Nils Risgaard-Petersen [d], Carina van der Veen [b], Sabine Kasten [e], Natascha Riedinger [f], Michael E. Böttcher [g], Thomas Röckmann [b], Bo Barker Jørgensen [d], Caroline P. Slomp [a]

[a] *Department of Earth Sciences – Geochemistry, Faculty of Geosciences, Utrecht University, The Netherlands*
[b] *Institute for Marine and Atmospheric Research Utrecht (IMAU), Utrecht University, The Netherlands*
[c] *Laboratoire de Glaciologie, Université Libre de Bruxelles, Belgium*
[d] *Center for Geomicrobiology, Aarhus University, Denmark*
[e] *Geosciences – Marine Geochemistry, Alfred Wegener Institute, Helmholtz Centre for Polar and Marine Research, Bremerhaven, Germany*
[f] *Boones Pickens School of Geology, Oklahoma State University, Stillwater, OK, USA*
[g] *Geochemistry & Isotope Biogeochemistry Group, Marine Geology Department, Leibniz Institute for Baltic Sea Research, Warnemünde, Germany*

Received 20 October 2016; accepted in revised form 21 March 2017; Available online 27 March 2017

Abstract

Methane is a powerful greenhouse gas and its emission from marine sediments to the atmosphere is largely controlled by anaerobic oxidation of methane (AOM). Traditionally, sulfate is considered to be the most important electron acceptor for AOM in marine sediments. Recent evidence suggests, however, that AOM may also be coupled to the reduction of iron (Fe) oxides. In the Baltic Sea, the post-glacial transition from the Ancylus freshwater phase to the Littorina brackish/marine phase (A/L-transition) around 9–7 kyr BP (before present), resulted in the accumulation of organic-rich brackish/marine sediments overlying organic-poor limnic deposits rich in Fe oxides. Methane produced in the organic-rich layer diffuses into the lake sediments, thus allowing for the possible coupling between Fe oxide reduction and methane oxidation.

Here, we combine detailed geochemical analyses of the sediment and pore water retrieved from three sites that were drilled during the IODP Baltic Sea Paleoenvironment Expedition 347 with multicomponent diagenetic modeling to study the possible role of Fe-mediated AOM as a mechanism for the apparent Fe oxide reduction in the methane-bearing lake deposits below the A/L transition. Our results reveal a complex interplay between production, oxidation and transport of methane showing that besides organoclastic Fe reduction, oxidation of downward migrating methane with Fe oxides may also explain the elevated concentrations of dissolved ferrous Fe in deep Baltic Sea sediments. Our findings imply that the transition of a lake toward a marine system could lead to reactivation of deeply buried, mostly crystalline Fe oxides in organic-poor lake deposits through reactions with downward diffusing methane from the overlying organic-rich marine sediments. Based on the geochemical profiles and numerical modeling, we propose that a potential coupling between Fe oxide reduction and methane oxidation likely affects deep Fe cycling and related biogeochemical processes, such as burial of phosphorus, in systems subject to changes in organic matter loading or bottom water salinity.

Keywords: Iron reduction; Methane; Marine sediments; Baltic Sea

* Corresponding author at: Center for Geomicrobiology, Aarhus University, Denmark.
E-mail address: egger@bios.au.dk (M. Egger).

http://dx.doi.org/10.1016/j.gca.2017.03.019
0016-7037/

1. INTRODUCTION

Methane (CH_4) is a powerful greenhouse gas in the Earth's atmosphere, generating 28–34 times more radiative forcing than carbon dioxide (CO_2) on a centennial time scale (Myhre et al., 2013). A major part of the CH_4 on Earth is produced in marine sediments by methanogenesis, which is the final step in the gradual fermentation of organic matter deposited on the seafloor. Despite high rates of CH_4 production in continental shelf and slope environments, the ocean today contributes only little CH_4 to the global atmospheric budget (Reeburgh, 2007). The small CH_4 efflux from the ocean to the atmosphere is largely due to the effective biological removal of pore water CH_4 through anaerobic oxidation with sulfate (SO_4^{2-}) in marine sediments (Niewöhner et al., 1998; Reeburgh, 2007; Knittel and Boetius, 2009):

$$CH_4 + SO_4^{2-} \rightarrow HS^- + HCO_3^- + H_2O \quad (I)$$

This reaction is most likely performed by syntrophic consortia of methanotrophic archaea and SO_4^{2-} reducing bacteria (Hoehler et al., 1994; Hinrichs et al., 1999; Boetius et al., 2000; Reeburgh, 2007; Knittel and Boetius, 2009) and may involve various possible cooperative metabolic strategies (Hoehler et al., 1994; Moran et al., 2008; Meyerdierks et al., 2010; Milucka et al., 2012; McGlynn et al., 2015; Wegener et al., 2015; Scheller et al., 2016). However, despite its global importance, the pathways and the factors that control the rates of anaerobic oxidation of CH_4 coupled to SO_4^{2-} reduction (SO_4-AOM) remain enigmatic.

Some anaerobic CH_4 oxidizing archaea known as ANME-2 have recently been shown to oxidize CH_4 nonsyntrophically using soluble Fe^{3+} complexes and nanoparticulate forms of Fe^{3+} as the electron acceptors (Ettwig et al., 2016; Scheller et al., 2016). The large multihaem cytochromes (proteins mediating electron transport) in the genomes of ANME-2 archaea indicate that these organisms should also be able to respire solid Fe oxides through extracellular electron transfer involving conductive cytochromes and/or so-called pili appendages. This is in accordance with recent geochemical evidence for Fe-mediated AOM (Fe-AOM) from field studies in a variety of aquatic environments (Beal et al., 2009; Sivan et al., 2011; Crowe et al., 2011; Amos et al., 2012; Wankel et al., 2012; Segarra et al., 2013; Riedinger et al., 2014; Egger et al., 2015b, 2016a), where the following reaction is proposed (Beal et al., 2009):

$$CH_4 + 8Fe(OH)_3 + 15H^+ \rightarrow HCO_3^- + 8Fe^{2+} + 21H_2O \quad (II)$$

Recent work further revealed that Fe oxides may stimulate SO_4-AOM (Sivan et al., 2014). In this mechanism, Fe oxides enhance the recycling of sulfide to SO_4^{2-} in a cryptic sulfur (S) cycle, where dissolved sulfide is oxidized to elemental sulfur (S^0). Subsequent disproportionation of S^0 to SO_4^{2-} and sulfide then fuels SO_4^{2-}-driven AOM by providing additional pore water SO_4^{2-} (Holmkvist et al., 2011a; Milucka et al., 2012; Treude et al., 2014; Sivan et al., 2014; Egger et al., 2016a). In addition, the presence of methanogens that are able to rapidly switch between methanogenesis and reduction of Fe oxides could result in the reduction of less reactive Fe oxides at depth in the sediment (Vargas et al., 1998; Bond and Lovley, 2002; Bodegom et al., 2004; Reiche et al., 2008; Liu et al., 2011; Oni et al., 2015; Sivan et al., 2016). The apparent coupling between CH_4 oxidation and Fe reduction previously observed could thus also be, at least partly, the result of indirect Fe stimulated SO_4-AOM and/or Fe oxide reduction by methanogens.

Regardless of the underlying mechanisms, Fe-associated pathways for CH_4 oxidation are of general interest not only because of the strong global warming potential of CH_4 in the Earth's atmosphere, but also because of the potential impacts on the marine Fe, S and phosphorus (P) cycles (März et al., 2008; Slomp et al., 2013; Hsu et al., 2014; Riedinger et al., 2014; Egger et al., 2015a; Rooze et al., 2016), and the diagenetic overprint of paleo-geochemical signals (Neretin et al., 2004; Jørgensen et al., 2004; Riedinger et al., 2005; Egger et al., 2016a). Environmental conditions that favor Fe-AOM in marine systems are still poorly understood. The required co-occurrence of pore water CH_4 and abundant reducible Fe oxides suggests that sediments receiving a relatively high input of Fe oxides compared to the in-situ production of sulfide may facilitate Fe-AOM. Rapid sediment accumulation could further reduce the exposure time of Fe oxides to dissolved sulfide, thus allowing a portion of the Fe oxides to escape the conversion to authigenic Fe sulfides and to remain preserved in the methanogenic sediments below the zone of SO_4^{2-} reduction and even below the zone of free sulfide (Kasten et al., 1998; Riedinger et al., 2005, 2014; März et al., 2008; Slomp et al., 2013; Egger et al., 2015b, 2016b; Rooze et al., 2016). In addition, perturbations inducing transient diagenesis such as anthropogenic eutrophication, climate change, and in particular post-glacial sea-level rise may also result in the burial of Fe oxide-rich deposits below sulfidic sediment layers (Boesen and Postma, 1988; Middelburg, 1991; Böttcher and Lepland, 2000; Neretin et al., 2004; Jørgensen et al., 2004; Riedinger et al., 2014; Egger et al., 2015b, 2016a; Rooze et al., 2016).

The Baltic Sea represents one of the world's largest brackish water bodies and is a dynamic ecosystem that has undergone many environmental changes since the last deglaciation of Scandinavia started 17–15 kyr before present (BP) (Björck, 1995; Andrén et al., 2000). One of the most pronounced transitions during the Holocene history of the Baltic Sea is the shift from the freshwater Ancylus Lake to the Littorina brackish/marine phase (A/L transition) 9–7 kyr BP (Sohlenius et al., 2001; Zillén et al., 2008). The resulting brackish/marine conditions led to the sedimentation of organic-rich sediments on top of organic-poor clay deposits, thereby driving a net downward diffusion of dissolved CH_4 into the Fe oxide-rich limnic deposits (Holmkvist et al., 2011a, 2014; Mogollón et al., 2012). The shift from a freshwater lake to a brackish/-marine environment during the Holocene and its associated transitional diagenetic state therefore make the Baltic Sea a suitable system to study the fate of sedimentary CH_4 in Fe oxide-rich and SO_4^{2-}-depleted systems.

The limnic clay, containing small amounts of SO_4^{2-} as a remnant of the seawater solutes that diffused into the freshwater deposits during the early A/L transgression, has been shown to act as a sink for the CH_4 produced in the Littorina sediments through SO_4-AOM (Mogollón et al., 2012; Holmkvist et al., 2014). If occurring, Fe-AOM could represent an additional, yet unrecognized, sink for CH_4 and a possible mechanism for the elevated pore water concentrations of ferrous iron (Fe^{2+}) previously reported in the Baltic Sea freshwater deposits (Holmkvist et al., 2011a, 2014; Dijkstra et al., 2016).

In this study, we discuss possible mechanisms responsible for the apparent Fe reduction in the limnic sediments below the A/L transition with a main focus on the potential role of AOM, using geochemical analyses and multicomponent diagenetic modeling of sediment cores obtained during the Integrated Ocean Drilling Program (IODP) Baltic Sea Paleoenvironment Expedition 347. Our results reveal a complex interplay between CH_4 production, oxidation and transport of CH_4 and indicate that at least part of the CH_4 generated in the brackish/marine deposits could be consumed by Fe-AOM within the underlying limnic clay, thus explaining part of the observed release of dissolved Fe^{2+} at depth.

2. STUDY SITES AND METHODS

2.1. Site description

Sediment cores from three different sites, M0065 (Bornholm Basin; 55°28.09′N, 15°28.63′E), M0063 (Landsort Deep; 58°37.34′N, 18°15.25′E) and M0059 (Little Belt; 55°0.29′N, 10°6.49′E), were collected during IODP Expedition 347 onboard the Greatship Manisha in 2013 (Fig. 1). Because of potential mustard gas contamination, the upper ca. 3 m of sediment at Site M0065 was not sampled. Changes in the abundance and diversity of diatoms and benthic foraminifera suggest the A/L-transition to be located at sediment depths of ~9–10 m at Site M0065, ~27 m at Site M0063 and ~48 m at Site M0059 (Andrén et al., 2015). At Site M0063, sediments deposited at ~50 m depth coincide with the partly brackish Yoldia Sea phase (Andrén et al., 2015), which formed after the final drainage of the Baltic Ice Lake (ca. 11.6–10.7 kyr BP) and which preceded the freshwater Ancylus Lake phase (ca. 10.7–10.0 kyr BP) (Zillén et al., 2008).

For Sites M0065 and M0059, the mid-composite depth (mcd) scales were used to compare sediment samples from different holes, whereas data for Site M0063 is presented in meters below seafloor (mbsf), since a stratigraphic correlation was not successful for the latter (Andrén et al., 2015).

2.2. Pore water analysis

Pore water was extracted immediately on recovery, using either Rhizon samplers or squeezers, and was subsampled under nitrogen for total sulfide, major cations and trace elements, alkalinity, ammonium (NH_4^+), dissolved inorganic carbon (DIC), stable water isotopes and for anions according to IODP standard procedures (Andrén et al., 2015). A 5 cm^3 sediment sample was collected onboard with a cut-off disposable syringe from the freshly

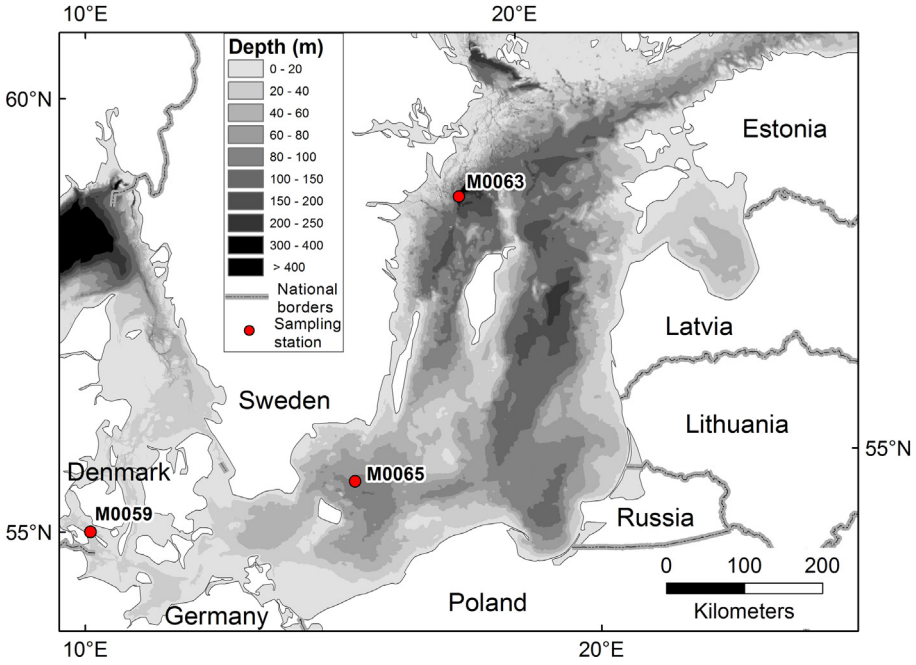

Fig. 1. Location of Baltic Sea study sites. Coring Sites M0065 (Bornholm Basin; 87 m water depth), M0063 (Landsort Deep; 451 m water depth) and M0059 (Little Belt; 37 m water depth) of the IODP Baltic Sea Paleoenvironment Expedition 347 are indicated by red points (map provided by Erik Smedberg, Stockholm University). (For interpretation of the references to colour in this figure legend, the reader is referred to the web version of this article.)

exposed end of every 1.5 m long core section and analyzed for pore water CH_4 following standard IODP protocols for headspace sampling and analysis. $\delta^{13}C$-CH_4 and δD-CH_4 (D, deuterium) were analyzed by a Continuous Flow Isotope Ratio Mass Spectrometry (CF-IRMS) system at the Institute for Marine and Atmospheric Research Utrecht (IMAU) (Brass and Röckmann, 2010; Sapart et al., 2011; Egger et al., 2015b). Additional CH_4 samples from Sites M0059 and M0065 were analyzed for $\delta^{13}C$-CH_4 at Aarhus University on a Gasbench II (Thermo Fisher Scientific, Bremen, Germany) coupled to a DELTA V plus IRMS (Thermo Fisher Scientific, Bremen, Germany), via Trace Gas Pre-Concentrator (PreCon; Thermo Fisher Scientific, Bremen, Germany) according to (Rice et al., 2001), and calibrated against an internal CH_4 standard having a delta value of −39.41‰ against VPDB (Vienna Pee Dee Belemnite). Samples from Site M0063 (Hole E) were also analyzed for $\delta^{13}C$-CH_4 at the Alfred Wegener Institute in Bremerhaven on a Delta Plus XP (Thermo Fisher Scientific, Bremen, Germany) via Pre-Concentrator (PreCon; Thermo Fisher Scientific, Bremen, Germany) and calibrated against standards T-IS03, L-IS01 and B-IS01 (Isometric Instruments). Overall, the standard deviation (1σ) for replicate measurements was <0.5‰ for $\delta^{13}C$-CH_4 and <2.6‰ for δD-CH_4.

DIC samples were poisoned with saturated $HgCl_2$ and subsequently analyzed using an AS-C3 analyzer (Apollo SciTech), consisting of an acidification and purging unit in combination with a LICOR-7000 CO_2/H_2O Gas Analyzer. The stable carbon isotope composition of DIC at Site M0063 was determined on a Gasbench II (Thermo Fisher Scientific, Bremen, Germany) coupled to a Delta V plus IRMS (Thermo Fisher Scientific, Bremen, Germany), according to (Torres et al., 2005) at Aarhus University. Samples from Sites M0059 and M0065 were analyzed for $\delta^{13}C$-DIC on a GasBench-II coupled to a Delta-V gas mass spectrometer (Thermo-Finnigan) at Utrecht University. The DIC carbon isotope composition is reported in delta notation relative to VPDB, on a scale normalized by assigning consensus values of −46.6‰ to the reference material L-SVEC lithium carbonate and +1.95‰ to the reference material NBS-19 calcium carbonate (Coplen et al., 2006). Both materials were used as internal standards during the analysis for all three sites. The precision for $\delta^{13}C$-DIC was better than ±0.4‰.

Stable hydrogen isotope measurements (D/H) on pore water samples stored after onboard sampling in glass vials were conducted by means of cavity ring-down spectroscopy (CRDS) (Picarro L2140-i) at Leibniz IOW, with a reproducibility of better than ±0.4‰. Note that values of δD-H_2O as well as dissolved SO_4^{2-} and Cl^- concentrations from depths between ~50 and 70 m at Site M0063 (Hole E) are not shown due to contamination of the samples with seawater during drilling, but all data are given in the Electronic Annex.

2.3. Bulk sediment analysis

Sediment samples were freeze dried, powdered and ground in an agate mortar inside an argon-filled glove box. An aliquot of ~125 mg of freeze-dried sediment was dissolved overnight in 2.5 mL HF (40%) and 2.5 mL of $HClO_4/HNO_3$ mixture, in a closed Teflon bomb at 90 °C. The acids were then evaporated at 140 °C (not to complete dryness) and the resulting gel was dissolved overnight in 1 M HNO_3 at 90 °C. Total elemental concentrations in the 1 M HNO_3 solutions were determined by ICP-OES (PerkinElmer Optima 3000 inductively coupled plasma-optical emission spectroscopy). Total organic carbon (TOC) was analyzed by the IODP onshore science party using a LECO CS-300 carbon-sulfur analyzer. Additional samples were analyzed at Utrecht University using an elemental analyzer (Fison Instruments model NA 1500 NCS) after carbonate removal from the sediment with two washes with 1 M HCl (4 h and 12 h) followed by two washes with Milli-Q water and subsequent drying of the samples (Van Santvoort et al., 2002).

Organic carbon isotope measurements were performed on 20–25 mg of decarbonized samples. To ensure complete carbonate removal, samples were placed in silver capsules treated with a few drops of HCl and subsequently oven dried at 40 °C and wrapped in tin capsules. Isotopic ratios were measured using a Thermo Finnigan Delta Plus XL isotope ratio mass spectrometer (IRMS) interfaced to a Costech ECS 4010 elemental analyzer (EA) at Oklahoma State University. Carbon isotope delta values ($\delta^{13}C$) are reported relative to VPDB and calculated using two isotopic standards (USGS 40 and USGS 24). The standard deviation (1σ) for replicate measurements was better than 0.3‰.

Anoxic sediment samples were collected onboard immediately upon core retrieval to investigate the redox-sensitive solid-phase partitioning of Fe. A 50 mg aliquot of freeze-dried (under vacuum) anoxic sediment was subjected to a sequential extraction procedure for Fe after (Poulton and Canfield, 2005). Sediment Fe was fractionated into carbonate associated Fe (Fe_{carb}; including siderite and ankerite), easily reducible (amorphous) oxides (Fe_{ox1}; including ferrihydrite and lepidocrocite) and reducible (crystalline) oxides (Fe_{ox2}; including goethite, hematite and akagenéite). Another 0.5 g aliquot of freeze-dried anoxic sediment was used to sequentially determine the amount of FeS (acid volatile sulfide, AVS) and FeS_2 (chromium reducible sulfur, CRS) via the diffusion-based approach described by (Burton et al., 2008).

2.4. Diagenetic modeling

2.4.1. General description

A 1-dimensional reactive transport model was developed for Site M0063 to investigate the potential for Fe-AOM as a source of pore water Fe^{2+} in the deep Baltic Sea sediments. The model describes the temporal evolution of 24 species (Table 1) via a set of mass conservation equations, which include physical transport as well as biogeochemical transformations (Reed et al., 2011b, 2011a). The generic form for solids and solutes is, respectively,

$$\frac{\partial C_S}{\partial t} = \frac{1}{(1-\phi)}\frac{\partial}{\partial x}(-v(1-\phi)C_s) + \sum R_S \qquad \text{(III)}$$

Table 1
Chemical species included in the diagenetic model.

Species	Notation	Type
Organic matter[a]	$OM^{\alpha,\beta,\gamma}$	Solid
Iron oxides[a]	$Fe(OH)_3^{\alpha,\beta,\gamma}$	Solid
Iron oxide-bound phosphorus	$Fe_{ox}P$	Solid
Iron monosulfide	FeS	Solid
Pyrite	FeS_2	Solid
Siderite	$FeCO_3$	Solid
Elemental sulfur	S^0	Solid
Vivianite	$Fe_3(PO_4)_2$	Solid
Apatite	$Ca_5(PO_4)_3OH$	Solid
Chloride	Cl^-	Solute
Calcium	Ca^{2+}	Solute
Oxygen	O_2	Solute
Sulfate	SO_4^{2-}	Solute
Iron	Fe^{2+}	Solute
Hydrogen sulfide[b]	$\sum H_2S$	Solute
Methane	CH_4	Solute
Ammonia and ammonium[b]	$\sum NH_4^+$	Solute
Nitrate	NO_3^-	Solute
Phosphate	$\sum PO_4^{3-}$	Solute
Dissolved inorganic carbon	DIC	Solute

[a] There are three types of species: reactive (α), less reactive (β) and refractory (γ).
[b] $\sum$ denotes that all species of an acid are included.

$$\frac{\partial C_{aq}}{\partial t} = \frac{1}{\phi}\frac{\partial}{\partial x}\left(D'\phi\frac{\partial C_{aq}}{\partial x} - u\phi C_{aq}\right) + \sum R_{aq} \quad \text{(IV)}$$

where C_S is the concentration of the solid species (mol cm^{-3}; mass per unit volume of solids), C_{aq} is the concentration of the solute (mol cm^{-3}; mass per unit volume of pore water), t is time (yr), ϕ is sediment porosity, x is distance from the sediment-water interface (cm), D' is the respective molecular diffusion coefficient in the sediment (D_m; $cm^2\ yr^{-1}$) at in situ conditions (Soetaert et al., 2010) and corrected for tortuosity (θ^2; Table S1; Boudreau, 1996), v and u are the advective burial velocities (cm yr^{-1}) of the solid phase and pore water, respectively, and $\sum R_S$ and $\sum R_{aq}$ are the net reaction rates (mol $cm^{-3}\ yr^{-1}$) per volume of solids and pore water, respectively. Porosity and advective velocities were described by depth-dependent functions assuming steady-state sediment compaction (Supplementary Tables S1 and S2, and Supplementary Fig. S1; Boudreau, 1997; Meysman et al., 2005).

Biogeochemical reactions implemented in the model and their corresponding rate laws are given in Tables 2 and 3, respectively. Corresponding reaction parameters were taken from literature. Where parameters were not available or no fit to the data could be obtained with existing parameter ranges they were constrained using the model (Table 4). Both Fe oxides and organic matter are divided into highly reactive (α), less reactive (β) and inert (γ) phases. The β phase of the Fe oxides is assumed to be less reactive towards dissolved sulfide than the α phase and, in contrast to the α phase, cannot be used by organoclastic Fe reduction (Egger et al., 2016a; Rooze et al., 2016). The latter assumption was made to test whether Fe-AOM alone could explain the apparent Fe reduction at depth and to allow an assessment of the potential impact of Fe-AOM on sedimentary CH_4 cycling. Note that the modeled Fe oxide phases do not directly relate to the operationally defined pools of Fe oxides. The model includes authigenic formation of Fe sulfides, Fe carbonates (siderite; $FeCO_3$) and vivianite ($Fe_3(PO_4)_2$) to account for sinks of pore water Fe^{2+}, assuming second-order kinetics (Egger et al., 2016a; Rooze et al., 2016) as well as apatite ($Ca_5(PO_4)_3OH$) formation and linear adsorption of NH_4^+ (Mackin and Aller, 1984; Soetaert and Herman, 2009). A model sensitivity analysis for key parameters is provided in the Supplementary Information (Supplementary Figs. S2–S4).

The model code was written in R (version 3.3.1) using the *marelac* package (Soetaert et al., 2010) for chemical and physical constants and the calculation of diffusion coefficients. Physical transport was calculated with the *ReacTran* package (Soetaert and Meysman, 2012). The depth domain, which describes the upper 100 m of the sediment, was separated into 1000 layers. While the upper layer was set at a thickness of 0.1 cm, that of the following grid layers increased exponentially to 37 cm at 100 m depth in the sediment. The set of equations obtained upon discretization of the mass conservation equations was solved with the lsoda ordinary differential equation solver (Hindmarsh, 1983; Petzoldt, 1983).

2.4.2. Initial and boundary conditions

Boundary conditions at the sediment–water interface were described as concentrations for the solutes and fluxes for the solids (Supplementary Table S3). At the lower boundary, a zero-gradient boundary condition was applied to all species. The model was run transiently to represent sediment accumulation over the past 25 kyr, assuming no changes in environmental conditions or fluxes before 13 kyr BP. Sediment burial rates before and after the onset of the A/L-transition were set constant at 0.42 and 0.35 cm yr^{-1}, respectively (corresponding to a A/L-transition at 8 kyr BP estimated by Zillén et al., 2008). The flux of organic matter entering the sediment was fit to the observed TOC profile, assuming (i) that the increase in organic matter loading at the A/L-transition coincided with the change in sedimentation rate; and (ii) that in the Littorina Sea sediments the ratio of the various organic matter fractions obeyed the multi-G model as determined for fresh planktonic material, i.e. 50% highly reactive, 16% less reactive and 34% refractory organic matter (Westrich and Berner, 1984) (Fig. 2). Changes in sedimentary Fe input after the A/L-transition follow the transient evolution of organic matter loading (Lenz et al., 2015). Iron oxides enter the sediment mostly in crystalline form (γ-phase) before 13 kyr BP and in more reactive form (α-phase) from 10 kyr BP onwards. Thus, Fe oxides deposited during the Baltic Ice Lake, i.e. below 50 m depth in the sediment (Andrén et al., 2015), are assumed to be unreactive. During the Holocene Thermal Maximum (HTM; 8–4.4 kyr BP) and Medieval Climate Anomaly (MCA; 1.7–0.8 kyr BP), periods of high productivity and widespread anoxia (Zillén et al., 2008; Jilbert and Slomp, 2013), we assume that part of the Fe oxides converted to pyrite before settling onto the sediment surface (Fig. 2). Bottom-water concentrations of sulfide are zero except during the MCA

Table 2
Reaction pathways and associated stoichiometries implemented in the diagenetic model (based on Reed et al., 2011a, 2011b; Egger et al., 2016a).

Primary redox reactions[a,b]	
$OM^{\alpha,\beta} + aO_2 \rightarrow aCO_2 + bNH_4^+ + cH_3PO_4 + aH_2O$	R1
$OM^{\alpha,\beta} + \frac{4a}{5}NO_3^- + \frac{4a}{5}H^+ \rightarrow aCO_2 + bNH_4^+ + cH_3PO_4 + \frac{2a}{5}N_2 + \frac{7a}{5}H_2O$	R2
$OM^{\alpha,\beta} + 4aFe(OH)_3^{\alpha} + 4a\chi Fe_{ox}P + 12aH^+ \rightarrow aCO_2 + bNH_4^+ + (c + 4a\chi)H_3PO_4 + 4aFe^{2+} + 13aH_2O$	R3
$OM^{\alpha,\beta} + \frac{a}{2}SO_4^{2-} + aH^+ \rightarrow aCO_2 + bNH_4^+ + cH_3PO_4 + \frac{a}{2}H_2S + aH_2O$	R4
$OM^{\alpha,\beta} \rightarrow \frac{a}{2}CO_2 + bNH_4^+ + cH_3PO_4 + \frac{a}{2}CH_4$	R5
Secondary redox and other reaction equations[b]	
$2O_2 + NH_4^+ + 2HCO_3^- \rightarrow NO_3^- + 2CO_2 + 3H_2O$	R6
$O_2 + 4Fe^{2+} + 8HCO_3^- + 2H_2O + 4\chi H_2PO_4^- \rightarrow 4Fe(OH)_3^{\alpha} + 4\chi Fe_{ox}P + 8CO_2$	R7
$2O_2 + FeS \rightarrow SO_4^{2-} + Fe^{2+}$	R8
$7O_2 + 2FeS_2 + 2H_2O \rightarrow 4SO_4^{2-} + 2Fe^{2+} + 4H^+$	R9
$2O_2 + H_2S + 2HCO_3^- \rightarrow SO_4^{2-} + 2CO_2 + 2H_2O$	R10
$2O_2 + CH_4 \rightarrow CO_2 + 2H_2O$	R11
$2Fe(OH)_3^{\alpha} + 2\chi Fe_{ox}P + H_2S + 4CO_2 \rightarrow 2Fe^{2+} + 2\chi H_2PO_4^- + S^0 + 4HCO_3^- + 2H_2O$	R12
$2Fe(OH)_3^{\beta} + 2\chi Fe_{ox}P + H_2S + 4CO_2 \rightarrow 2Fe^{2+} + 2\chi H_2PO_4^- + S^0 + 4HCO_3^- + 2H_2O$	R13
$Fe^{2+} + H_2S \rightarrow FeS + 2H^+$	R14
$FeS + H_2S \rightarrow FeS_2 + H_2$	R15
$4S^0 + 4H_2O \rightarrow 3H_2S + SO_4^{2-} + 2H^+$	R16
$FeS + S^0 \rightarrow FeS_2$	R17
$SO_4^{2-} + CH_4 + CO_2 \rightarrow 2HCO_3^- + H_2S$	R18
$CH_4 + 8Fe(OH)_3^{\alpha,\beta} + 8\ \chi Fe_{ox}P + 15H^+ \rightarrow HCO_3^- + 8Fe^{2+} + 8\chi H_2PO_4^- + 21H_2O$	R19
$Fe(OH)_3^{\alpha} + \chi Fe_{ox}P \rightarrow Fe(OH)_3^{\beta} + \chi H_2PO_4^-$	R20
$Fe(OH)_3^{\beta} + \chi Fe_{ox}P \rightarrow Fe(OH)_3^{\gamma} + \chi H_2PO_4^-$	R21
$3Fe^{2+} + 2HPO_4^- \rightarrow Fe_3(PO_4)_2 + 2H^+$	R22
$Fe^{2+} + CO_3^{2-} \rightarrow FeCO_3$	R23
$5Ca^{2+} + 3PO_4^{3-} + H_2O \rightarrow Ca_5(PO_4)_3OH + H^+$	R24

R6 = nitrification; R7 = $Fe(OH)_3$ formation; R8 = FeS oxidation; R9 = FeS_2 oxidation; R10 = H_2S oxidation; R11 = aerobic CH_4 oxidation; R12 and R13 = $Fe(OH)_3$ reduction by H_2S; R14 = FeS formation; R15 = FeS_2 formation (H_2S pathway); R16 = S^0 disproportionation; R17 = FeS_2 formation (polysulfide pathway); R18 = SO_4-AOM; R19 = Fe-AOM; R20 = conversion (i.e. crystallization) from α to β phase; R21 = crystallization from β to γ phase; R22 = vivianite formation, R23 = siderite precipitation and R24 = apatite formation.

[a] Organic matter (OM) is of the form $(CH_2O)_a(NH_4^+)_b(H_3PO_4)_c$, with 'a' = 1, 'b' = 16/106 and 'c' = 1/150. Before the A/L-transition (8 kyr BP), 'b' and 'c' were reduced by a factor of 15 to represent low-quality OM.

[b] χ refers to the P:Fe ratio of $Fe(OH)_3^{\alpha,\beta,\gamma}$.

and during the HTM. Bottom-water salinity conditions were varied such that a best fit to the observed pore water Cl^- profile was obtained.

3. RESULTS

3.1. Solid phase

The shift from a freshwater lake towards a brackish/marine depositional environment at the A/L-transition is characterized by a pronounced increase in sedimentary TOC and total S at all three study sites (Fig. 3). Compared to the Littorina Sea sediments, the limnic deposits are depleted in sedimentary S (<50 μmol g^{-1}), Fe sulfides (<50 μmol g^{-1}) and poor in organic carbon (~0.5 wt%), while containing high amounts of reducible Fe oxides (~200–300 μmol g^{-1} at Site M0065, ~200–350 μmol g^{-1} at Site M0063 and ~100–150 μmol g^{-1} at Site M0059). At Site M0063, slightly elevated contents of TOC and solid phase S are observed around ~40–50 m depth. Sedimentary Fe carbonates show a distinct peak of ~80 μmol g^{-1} below the A/L transition at Site M0065. Sites M0063 and M0059 display Fe carbonate contents of ~100 μmol g^{-1} and ~50 μmol g^{-1}, respectively, in the limnic deposits below the A/L transition.

The relative contribution of amorphous Fe oxides (Fe_{ox1}) to the total amount of Fe oxides declines from 47% around the A/L transition to ~20% around 15 m depth at Site M0065 (Fig. 4). Below 15 m depth, crystalline Fe oxides (Fe_{ox2}) become the dominant Fe oxide phase, accounting for ~80% of total Fe oxides. At Site M0059, the same pattern of a declining contribution of amorphous Fe oxides (from ~50% to ~30%) and an increase in the relative abundance of crystalline Fe oxides (from ~20% to ~50%) is observed in the sediments below the A/L transition. At Site M0063, in contrast, an almost equal contribution of amorphous and crystalline Fe oxides (~45%) is observed in the Fe^{2+}-rich sediments below the A/L transition, and the same shift toward a dominance of crystalline Fe oxides below a depth of ~50 m.

3.2. Pore water profiles

Pore water concentrations of alkalinity, NH_4^+ and DIC are highest in the organic-rich Littorina Sea sediments and indicate a net downward diffusive flux of these

Table 3
Reaction equations implemented in the model (based on Reed et al., 2011a, 2011b; Egger et al., 2016a).

Primary redox reaction equations	
$R_1 = k_{\propto,\beta} OM^{\propto,\beta} \left(\frac{[O_2]}{K_{O_2}+[O_2]}\right)$	(E1)
$R_2 = k_{\propto,\beta} OM^{\propto,\beta} \left(\frac{[NO_3^-]}{K_{NO_3^-}+[NO_3^-]}\right)\left(\frac{K_{O_2}}{K_{O_2}+[O_2]}\right)$	(E2)
$R_3 = k_{\propto,\beta} OM^{\propto,\beta} \left(\frac{[Fe(OH)_3^x]}{K_{Fe(OH)_3^x}+[Fe(OH)_3^x]}\right)\left(\frac{K_{NO_3^-}}{K_{NO_3^-}+[NO_3^-]}\right)\left(\frac{K_{O_2}}{K_{O_2}+[O_2]}\right)$	(E3)
$R_4 = \Psi k_{\propto,\beta} OM^{\propto,\beta} \left(\frac{[SO_4^{2-}]}{K_{SO_4^{2-}}+[SO_4^{2-}]}\right)\left(\frac{K_{Fe(OH)_3^x}}{K_{Fe(OH)_3^x}+[Fe(OH)_3^x]}\right)\left(\frac{K_{NO_3^-}}{K_{NO_3^-}+[NO_3^-]}\right)\left(\frac{K_{O_2}}{K_{O_2}+[O_2]}\right)$	(E4)
$R_5 = \Psi k_{\propto,\beta} OM^{\propto,\beta} \left(\frac{K_{SO_4^{2-}}}{K_{SO_4^{2-}}+[SO_4^{2-}]}\right)\left(\frac{K_{Fe(OH)_3^x}}{K_{Fe(OH)_3^x}+[Fe(OH)_3^x]}\right)\left(\frac{K_{NO_3^-}}{K_{NO_3^-}+[NO_3^-]}\right)\left(\frac{K_{O_2}}{K_{O_2}+[O_2]}\right)$	(E5)
Secondary redox and other reaction equations	
$R_6 = k_1[O_2][NH_4^+]$	(E6)
$R_7 = k_2[O_2][Fe^{2+}]$	(E7)
$R_8 = k_3[O_2][FeS]$	(E8)
$R_9 = k_4[O_2][FeS_2]$	(E9)
$R_{10} = k_5[O_2][\sum H_2S]$	(E10)
$R_{11} = k_6[O_2][CH_4]$	(E11)
$R_{12} = k_7[Fe(OH)_3^{\propto}][\sum H_2S]$	(E12)
$R_{13} = k_8[Fe(OH)_3^{\beta}][\sum H_2S]$	(E13)
$R_{14} = k_9[Fe^{2+}][\sum H_2S]$	(E14)
$R_{15} = k_{10}[FeS][\sum H_2S]$	(E15)
$R_{16} = k_{11}[S_0]$	(E16)
$R_{17} = k_{12}[FeS][S_0]$	(E17)
$R_{18} = k_{13}[SO_4^{2-}][CH_4]$	(E18)
$R_{19} = k_{14}[Fe(OH)_3^{\propto,\beta}][CH_4]$	(E19)
$R_{20} = k_{15}[Fe(OH)_3^{\propto}]$	(E20)
$R_{21} = k_{16}[Fe(OH)_3^{\beta}]$	(E21)
$R_{22} = k_{17}[Fe^{2+}][HPO_4^{2-}]$	(E22)
$R_{23} = k_{18}[Fe^{2+}][DIC]$	(E23)
$R_{24} = k_{19}[Ca^{2+}][HPO_4^{2-}]$	(E24)

constituents into the limnic deposits (Fig. 5). The concentrations of these key products of organic matter remineralization increase with increasing thickness of the Littorina deposits and TOC contents (M0065 < M0063 < M0059). At Site M0063, alkalinity and DIC display elevated concentrations at depth of 40–50 m coinciding with sediments with elevated TOC contents.

Concentrations of pore water SO_4^{2-} and dissolved sulfide indicate active SO_4^{2-} reduction above 5 m at Site M0065 and above 1.5 m at Site M0063, with pore waters depleted in SO_4^{2-} and sulfide below. Site M0059 shows variable SO_4^{2-} concentrations between 0 and 2 mM until a depth of around 50 m. Dissolved sulfide was only detected in the upper ~0.5 m of the sediment. However, SO_4^{2-} concentrations increase again around a depth of 17 m (M0065), 70 m (M0063) and 85 m (M0059), where values of ~0.4 mM, ~2 mM, and ~6 mM are reached, respectively.

At Site M0065, concentrations of pore water CH_4 are highest in the Littorina Sea deposits (~10 mM) and decrease with sediment depth (Fig. 5). However, it is important to note that due to extensive degassing observed during core recovery (Andrén et al., 2015), the measured concentrations of CH_4 are not all representative of actual CH_4 concentrations and should thus be viewed as an indicator of presence or absence rather than interpreted as absolute values. This is particularly the case for sites M0063 and M0059 (Andrén et al., 2015). Hence, most data in the CH_4 zone indicate high super-saturation of CH_4 most of which has been lost by degassing (indicated by white symbols in Figs. 5 and 7). Below a depth of ~20 m (M0065), ~40 m (M0063), and ~60 m (M0059), however, CH_4 concentrations consistently drop below 1 bar saturation and follow a smooth profile, suggesting that the measurements from the deeper parts of the sediment may reflect actual concentrations. Dissolved Fe^{2+} shows a distinct maximum in the methanogenic pore waters below the A/L transition at all three sites with concentrations of up to ~1 mM (M0065), ~0.6 mM (M0063), and ~1.5 mM (M0059).

3.3. Carbon and hydrogen isotopes

Organic matter at Sites M0065 and M0063 is generally depleted in ^{13}C and shows a small decrease in $\delta^{13}C$-TOC from ~−25‰ at the A/L transition to ~−28‰ at depth in the limnic deposits (Fig. 6). At Site M0059, values of $\delta^{13}C$-TOC are around ~−19‰ in the Littorina Sea sediments and sharply decrease to ~−27‰ below the A/L transition.

The Littorina Sea sediments are characterized by ^{13}C-enriched DIC, when compared to the underlying glacial clay, with values of $\delta^{13}C$-DIC of ~11‰ (M0065), ~17‰ (M0063) and ~25‰ (M0059) (Fig. 6). Below the A/L

Table 4
Reaction parameters used in the diagenetic model.

Parameter	Symbol	Value	Units	Values given in literature
Decay constant for OM^{α}	k_{α}	0.03	yr^{-1}	0.05–1.62[a,b]
Decay constant for OM^{β}	k_{β}	0.0025	yr^{-1}	0.0025–0.0086[b,h]
Limiting concentration of O_2	K_{O2}	20	$\mu mol\ L^{-1}$	1–30[c]
Limiting concentration of NO_3^-	K_{NO3}-	4	$\mu mol\ L^{-1}$	4–80[c]
Limiting concentration of $Fe(OH)_3$	$K_{Fe(OH)3}$	65	$\mu mol\ g^{-1}$	65–100[c]
Limiting concentration of SO_4^{2-}	K_{SO42-}	1.6	$mmol\ L^{-1}$	1.6[c]
Attenuation factor for E4 and E5	Ψ	0.0018	–	0.00157–0.075[b,d]
Rate constant for reaction E6	k_1	10,000	$mmol^{-1}\ L\ yr^{-1}$	50,00–39,000[c,d]
Rate constant for reaction E7	k_2	140,000	$mmol^{-1}\ L\ yr^{-1}$	140,000[c]
Rate constant for reaction E8	k_3	300	$mmol^{-1}\ L\ yr^{-1}$	300[c]
Rate constant for reaction E9	k_4	1	$mmol^{-1}\ L\ yr^{-1}$	1[c]
Rate constant for reaction E10	k_5	160	$mmol^{-1}\ L\ yr^{-1}$	≥160[c]
Rate constant for reaction E11	k_6	10^7	$mmol^{-1}\ L\ yr^{-1}$	10,000,000[c]
Rate constant for reaction E12	k_7	8	$mmol^{-1}\ L\ yr^{-1}$	≤100[c]
Rate constant for reaction E13	k_8	0.08	$mmol^{-1}\ L\ yr^{-1}$	0.95[i]
Rate constant for reaction E14	k_9	14,800	$mmol^{-1}\ L\ yr^{-1}$	100–14,800[b,d]
Rate constant for reaction E15	k_{10}	0.0003	$mmol^{-1}\ L\ yr^{-1}$	0.0003–3.15[e,i]
Rate constant for reaction E16	k_{11}	3	yr^{-1}	3[f]
Rate constant for reaction E17	k_{12}	7	$mmol^{-1}\ L\ yr^{-1}$	7[f]
Rate constant for reaction E18	k_{13}	7.5	$mmol^{-1}\ L\ yr^{-1}$	10[c]
Rate constant for reaction E19	k_{14}	$4.6 * 10^{-7}$	$mmol^{-1}\ L\ yr^{-1}$	$1.6 * 10^{-7}$–0.0074[g,i]
Rate constant for reaction E20	k_{15}	0.6	yr^{-1}	0.6[f]
Rate constant for reaction E21	k_{16}	0.000013	yr^{-1}	0.000013[i]
Rate constant for reaction E22	k_{17}	0.005	$mmol^{-1}\ L\ yr^{-1}$	0.052[i]
Rate constant for reaction E23	k_{18}	0.01	$mmol^{-1}\ L\ yr^{-1}$	0.0027[i]
Rate constant for reaction E24	k_{19}	0.000025	$mmol^{-1}\ L\ yr^{-1}$	Model constrained
Linear adsorption coefficient for NH_4^+	K_{NH4}	1.3	–	1.3[j]

[a] Moodley et al. (2005).
[b] Reed et al. (2011b).
[c] Wang and Van Cappellen (1996).
[d] Reed et al. (2011a).
[e] Rickard and Luther (1997).
[f] Berg et al. (2003).
[g] Rooze et al. (2016).
[h] Reed et al. (2016).
[i] Egger et al. (2016a).
[j] Mackin and Aller (1984).

transition, δ^{13}C-DIC shows a shift to more ^{13}C-depleted DIC with values of ~−20‰ at all sites. However, while δ^{13}C-DIC generally stays constant below the zone with elevated Fe^{2+} concentrations at Site M0063 and M0059, it increases again below ~35 m depth at Site M0065.

The smooth pore water profiles of δ^{13}C-CH_4 and δD-CH_4 suggest that the isotopic composition of dissolved CH_4 is not significantly affected by CH_4 degassing, consistent with earlier observations (Wallace et al., 2000; Egger et al., 2016a). Littorina Sea sediments are characterized by isotopically light CH_4 at all sites, with values of δ^{13}C-CH_4 ranging between ~−80‰ and −50‰ and δD-CH_4 between ~−250‰ and −220‰, respectively (Fig. 6). In the limnic deposits, dissolved CH_4 becomes less enriched in ^{13}C with depth. However, at Site M0063, CH_4 becomes progressively enriched in ^{13}C again below ~70 m depth. At Site M0065, δD-CH_4 displays only a slight depletion in the heavy isotope with depth and a distinct gradient change around 37 m towards isotopically lighter δD-CH_4. Pore water CH_4 at Site M0063 shows a gradual depletion in δD-CH_4 with depth, starting from ~−220‰ close to the sediment surface to ~−270‰ at 50–70 m depth in the limnic deposits. Below 70 m, δD-CH_4 increases steeply again with depth. Site M0059 shows a gradual depletion in δD-CH_4 with depth from ~−210‰ close to the sediment surface to ~−250‰ around 50 m depth, below which δD-CH_4 increases again towards higher values, before declining again even further. Pore water δD-H_2O decreases downward at all sites, from ~−40‰ to ~−130‰ at Sites M0065 and M0063, and from −20‰ to ~−90‰ at Site M0059, respectively.

3.4. Modeling results

In general, the modeled solid phase and pore water profiles for Site M0063 are in good agreement with the measured data, except for the Fe carbonate profile in the Littorina Sea sediments, a narrow peak of Fe oxides around ~7–9 m depth, and the pore water CH_4 concentrations (Fig. 7). Note, however, that the measured Fe carbonate and Fe oxide contents in the Littorina Sea deposits could be overestimated due to AVS dissolution during the Na

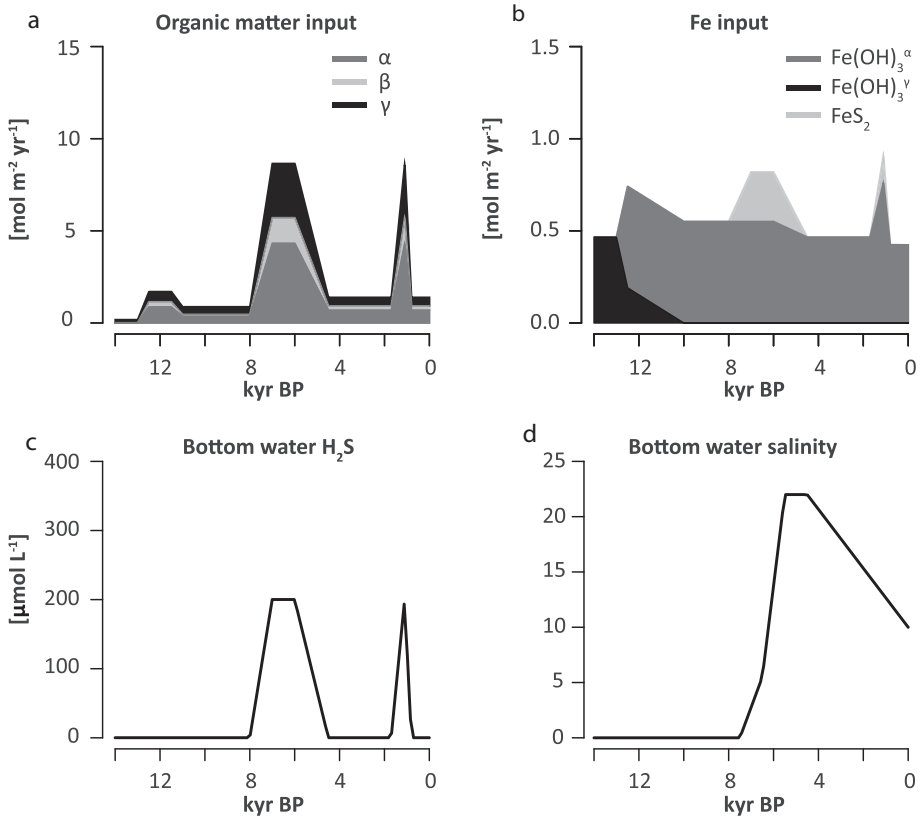

Fig. 2. Variations in (a) input of organic matter and (b) solid Fe species, as well as (c) changes in bottom water concentrations of sulfide and (d) bottom water salinity during the last 14 kyr of the model simulation. Inputs and environmental conditions before 13 kyr BP are constant. Timing of the peaks in Fe input after the A/L transition (b) and the timing of enhanced bottom water sulfide concentrations (c) are consistent with changes in organic matter loading. Note that α, β and γ refer to highly reactive, less reactive and inert phases of Fe oxides and organic matter, respectively. Also note that the β and γ phases of Fe oxides are formed in the sediments by conversion from α-Fe and β-Fe oxides, respectively (Table 2).

acetate and hydroxylamine-HCl extraction steps (Egger et al., 2015b). Concentrations of AVS are around ~30–300 µmol g^{-1} in the Littorina Sea sediments and <10 µmol g^{-1} in the limnic deposits (Supplementary Fig. S5). Furthermore, higher modeled concentrations of pore water CH_4 when compared to measured values are typical for sediments where strong degassing has been observed during core recovery (e.g. Arndt et al., 2006; Egger et al., 2016a). The elevated concentrations of dissolved SO_4^{2-} below ~70 m depth in the sediment could not be reproduced in the model. We note that this implies that the SO_4^{2-} cannot be a remnant of the seawater solutes that diffused into the freshwater deposits during the early A/L transgression.

Modeled present-day rates of CH_4 production show two distinct maxima of ~65 pmol CH_4 cm^{-3} d^{-1} and ~85 pmol CH_4 cm^{-3} d^{-1} in the organic-rich Littorina Sea sediments deposited during the MCA and during the HTM, respectively. In the limnic deposits, CH_4 production rates are <10 pmol CH_4 cm^{-3} d^{-1}. Anaerobic oxidation of CH_4 coupled to SO_4^{2-} reduction is restricted to the upper 3 m of sediment, with highest rates of ~740 pmol CH_4 cm^{-3} d^{-1} around 2 m depth in the sediment. Rates of Fe-AOM show peaks of ~3 pmol CH_4 cm^{-3} d^{-1} between ~10 and 20 m depth in the Littorina Sea sediments and of ~2.5 pmol CH_4 cm^{-3} d^{-1} at the A/L transition. Below the A/L transition, Fe-AOM rates decrease to <0.01 pmol CH_4 cm^{-3} d^{-1} around 60 m depth in the limnic deposits. S^0 disproportionation is constrained to the upper 3 m of sediment, with a maximum rate of ~2 pmol S^0 - cm^{-3} d^{-1} between 1 and 2 m depth.

Modeled depth-integrated rates of organoclastic SO_4^{2-} reduction, CH_4 production, SO_4-AOM and Fe-AOM are ~9.2 µmol SO_4^{2-} m^{-2} d^{-1}, ~846 µmol CH_4 m^{-2} d^{-1}, ~240 µmol CH_4 m^{-2} d^{-1} and ~31 µmol CH_4 m^{-2} d^{-1}, respectively, in the Littorina Sea sediments and 0 µmol SO_4^{2-} m^{-2} d^{-1}, ~105 µmol CH_4 m^{-2} d^{-1}, 0 µmol CH_4 m^{-2} d^{-1} and 37 µmol CH_4 m^{-2} d^{-1}, respectively, in the deposits below the A/L transition (>27 m depth).

4. DISCUSSION

4.1. CH_4 production in the sediment

The establishment of more productive brackish/marine conditions during the early Holocene resulted in a prominent transition from Fe oxide-rich clay to organic carbon-rich sediments at all three sites (Fig. 3), consistent

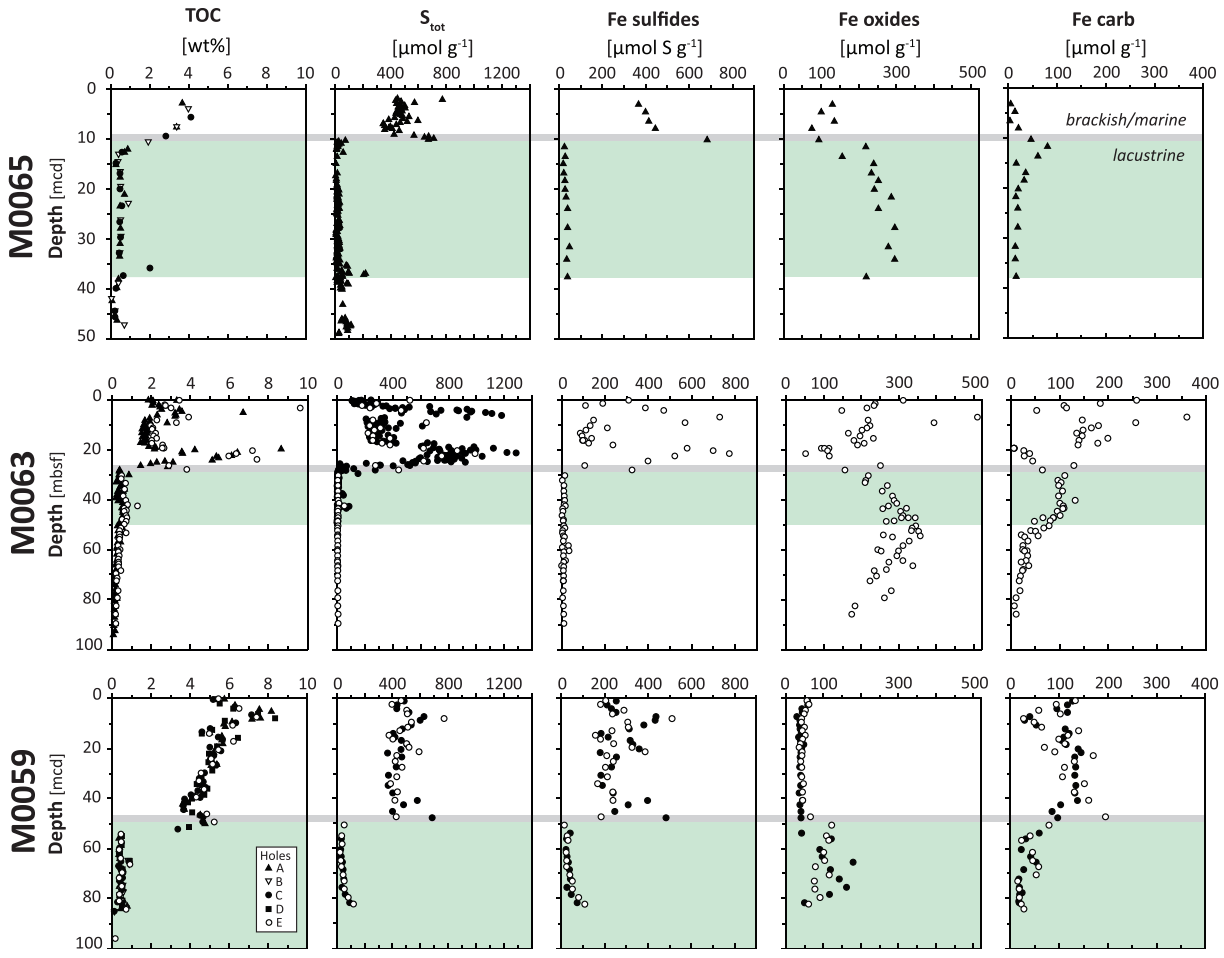

Fig. 3. Solid phase sediment profiles of total organic carbon (TOC), sulfur (S_{tot}), Fe sulfides (sum of AVS (acid volatile sulfide) and CRS (chromium reducible sulfur); see Supplementary Fig. S5), Fe oxides (sum of amorphous, crystalline and recalcitrant oxides, i.e. Fe_{ox1}, Fe_{ox2} and Fe_{magn}) and Fe carbonates (Fe carb). The gray bar indicates the transition from the Ancylus freshwater phase to the Littorina brackish/marine phase (A/L transition). The green shaded area indicates sediments with elevated concentrations of pore water Fe^{2+} below the A/L transition (see Fig. 5). Note the different depth scale for Site M0065. (For interpretation of the references to colour in this figure legend, the reader is referred to the web version of this article.)

with previously published Baltic Sea sediment records (Böttcher and Lepland, 2000; Holmkvist et al., 2014; Dijkstra et al., 2016). Pore water profiles of alkalinity and NH_4^+ indicate high rates of organic matter degradation in the Littorina Sea sediments (Fig. 5). Increasing concentrations of TOC, alkalinity and NH_4^+ between the sites and the observed degassing during sampling (M0065 < M0063 < M0059) points towards higher inputs and rates of organic matter remineralization and methanogenesis with increasing thickness of the Holocene brackish/marine deposits.

The isotopic composition of CH_4 can be used to identify the main source of pore water CH_4, as each type of CH_4 formation pathway produces a characteristic isotopic signature in $\delta^{13}C$ and δD (Whiticar, 1999). Co-isotope plots of pore water CH_4 reveal that hydrogenotrophic carbonate reduction, i.e. microbial reduction of CO_2 to CH_4, represents the main methanogenic pathway in the Littorina Sea sediments at all sites (Fig. 8). In the limnic deposits at Site M0063 and M0059, pore water CH_4 has a $\delta^{13}C$ and δD isotope signature typically associated with mixed or transitional systems, indicating a substrate shift from carbonate reduction to acetate fermentation - the dominant methanogenic pathway in organic-rich freshwater environments (Whiticar, 1999) - or to methylotrophic methanogenesis, and mixing with downward diffusing Littorina Sea-derived CH_4 (Fig. 8). Interestingly, CH_4 in the limnic deposits at Site M0065 shows an isotopic composition dominated by carbonate reduction. This is likely the result of thinner Littorina Sea deposits, which during the early A/L transgression allowed seawater SO_4^{2-} to diffuse deeper into the limnic deposits, thus stimulating competitive SO_4^{2-} reduction. Pore water CH_4 in the deep limnic deposits at Site M0063 and M0065 fall outside the range commonly determined for hydrogenotrophic methanogenesis using contemporary ocean water (Whiticar, 1999) (Fig. 8), which further indicates CO_2 reduction at depth using old D-depleted glacial water and ^{13}C-depleted DIC (i.e. CO_2) as substrates (Fig. 6). These results suggest that CH_4 in the sediments below the A/L transition is not only from

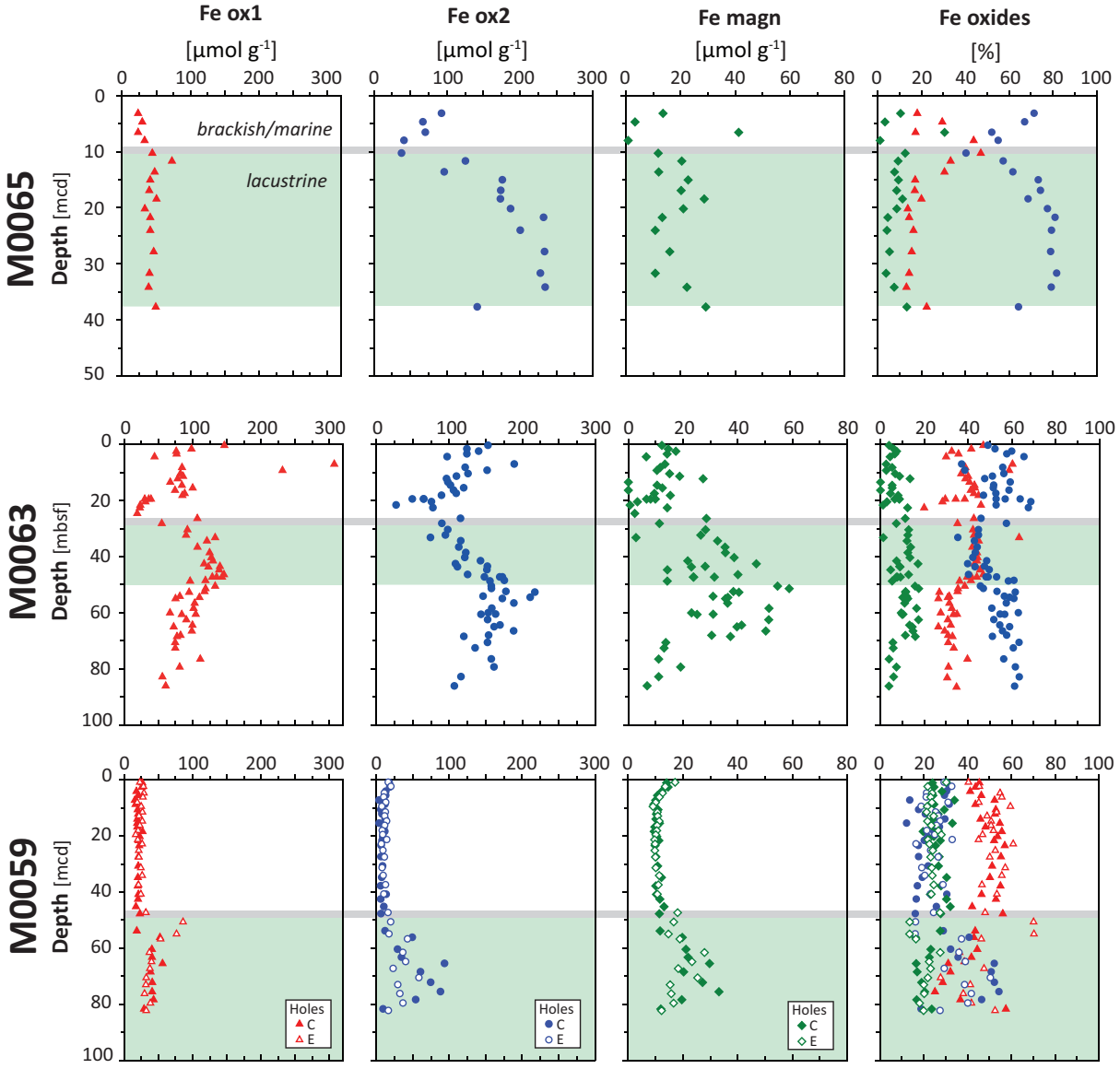

Fig. 4. Different Fe oxide fractions extracted using the procedure after (Poulton and Canfield, 2005), including easily reducible (amorphous) oxides ("Fe ox1"), reducible (crystalline) oxides ("Fe ox2") and magnetite ("Fe magn"), and their relative contribution to total Fe oxides. The gray bar and the green shaded area are explained in the legend of Fig. 3. Note that the amount of Fe ox1 is likely overestimated in Fe sulfide-rich Littorina Sea sediments due to potential AVS dissolution during the hydroxylamine-HCl extraction step (see Supplementary Fig. S5 for the AVS contents) (Egger et al., 2015b). Also note the different depth scale for Site M0065. (For interpretation of the references to colour in this figure legend, the reader is referred to the web version of this article.)

downward diffusion, but also partly from methanogenesis within the limnic deposits. Thus, the CH_4 at depth is a mixture of CH_4 diffusing downward from the Littorina Sea deposits and CH_4 produced at low rates in the limnic sediments.

The presence of dissolved CH_4 in the Fe oxide-rich freshwater deposits creates conditions favorable for a potential coupling between CH_4 oxidation and Fe oxide reduction through Fe-AOM. In the following, the possible role of Fe-AOM and of other feasible mechanisms responsible for Fe reduction in the limnic sediments below the A/L transition is discussed.

4.2. Organoclastic Fe reduction in methanogenic sediments

The sediments below the A/L transition, where pore water Fe^{2+} is abundant, contain significant amounts of poorly crystalline (amorphous) Fe oxides that account for ~30–40% of total Fe oxides at all three sites (Fig. 4). Such high contents of easily reducible Fe oxides could favor organoclastic Fe reduction, i.e. oxidation of organic matter coupled to the reduction of Fe oxides in these sediments. Several studies have documented that Fe-reducing organisms are able to outcompete methanogens for common substrates (e.g. acetate and hydrogen), reducing

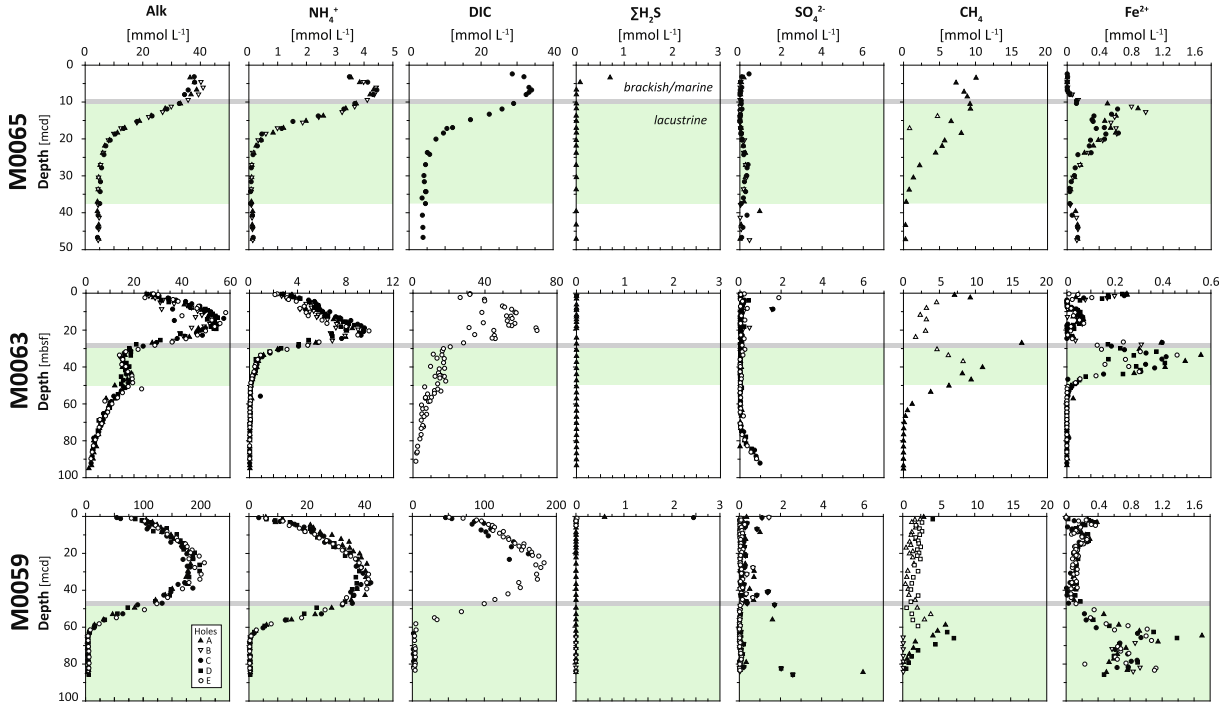

Fig. 5. Pore water profiles of alkalinity (Alk), NH_4^+, dissolved inorganic carbon (DIC), sulfide ($\sum H_2S = H_2S + HS^- + S^{2-}$), SO_4^{2-}, CH_4 and Fe^{2+}. The gray bar and the green shaded area are explained in the legend of Fig. 3. The white symbols for CH_4 indicate that these measurements represent the remains of CH_4 after most CH_4 has been lost due to outgassing during coring. Note the different depth scale for Site M0065 as well as the different scales on the x-axes between the sites. (For interpretation of the references to colour in this figure legend, the reader is referred to the web version of this article.)

the concentration of these primary electron donors to levels that are too low for methanogens to grow (Lovley and Phillips, 1987; Lovley et al., 1989; Achtnich et al., 1995). In addition, direct inhibition of methanogenesis by Fe oxides has been reported, where methanogens capable of Fe reduction drive a diversion of electron flow from CH_4 production to Fe reduction (Vargas et al., 1998; Bond and Lovley, 2002; Bodegom et al., 2004; Reiche et al., 2008; Liu et al., 2011; Sivan et al., 2016). Hence, organoclastic Fe reduction has commonly been proposed to exert a suppressive effect on CH_4 production. (Semi)conductive Fe oxides (e.g. hematite and magnetite) were recently reported to stimulate methanogenesis in laboratory incubation studies (Kato et al., 2012; Cruz Viggi et al., 2014; Li et al., 2014; Zhou et al., 2014; Zhuang et al., 2015). These studies proposed that (semi)conductive crystalline Fe oxides could serve as conduits between the electron-donating organoclastic Fe reducers and electron-accepting, CO_2 reducing methanogens via direct interspecies electron transfer, thus potentially allowing concurrent methanogenesis and organoclastic Fe reduction. The inhibitory effect of Fe reduction on methanogenesis thus appears to be lower for crystalline Fe oxides such as hematite and magnetite, which are less bioavailable to Fe reducing organisms than poorly crystalline (amorphous) Fe (oxyhydr)oxides (e.g. ferrihydrite and lepidocrocite) (Lovley, 1991; Qu et al., 2004; Zhuang et al., 2015). These findings reveal that the crystallinity and conductivity of Fe oxides play a key role in determining whether methanogenesis is stimulated or suppressed in Fe oxide-rich environments.

The increase in the relative contribution of crystalline Fe oxides below the A/L transition (Fig. 4) may therefore, in theory, allow a co-occurrence of methanogenesis and organoclastic Fe reduction in these sediments through direct interspecies electron transfer between Fe reducers and methanogens. Organoclastic Fe reduction could in fact also be occurring in the methanogenic sediments above the A/L transition thereby contributing to the observed accumulation of Fe^{2+} in the pore water. In this scenario, a high availability of organic matter would initially stimulate SO_4^{2-} reduction and sulfide-induced reduction of Fe oxides at the expense of organoclastic Fe reduction, shortly after deposition of the sediment. In case of a large surplus of reactive Fe(III) relative to SO_4^{2-}, the former may persist in the sediment upon burial below the zone of SO_4^{2-} reduction. The subsequent co-occurrence of organoclastic Fe reduction and methanogensis is in accordance with increasing evidence showing that the 'Froelich model' of the primary redox-reactions in aquatic sediments with a characteristic succession of different redox zones (Froelich et al., 1979) is less rigorous than commonly thought (Postma and Jakobsen, 1996; Bethke et al., 2011; Treude et al., 2014; Egger et al., 2016b; Sivan et al., 2016). However, it remains to be shown whether the old and refractory organic matter in the limnic clay is a suitable electron donor for Fe reducing microorganisms.

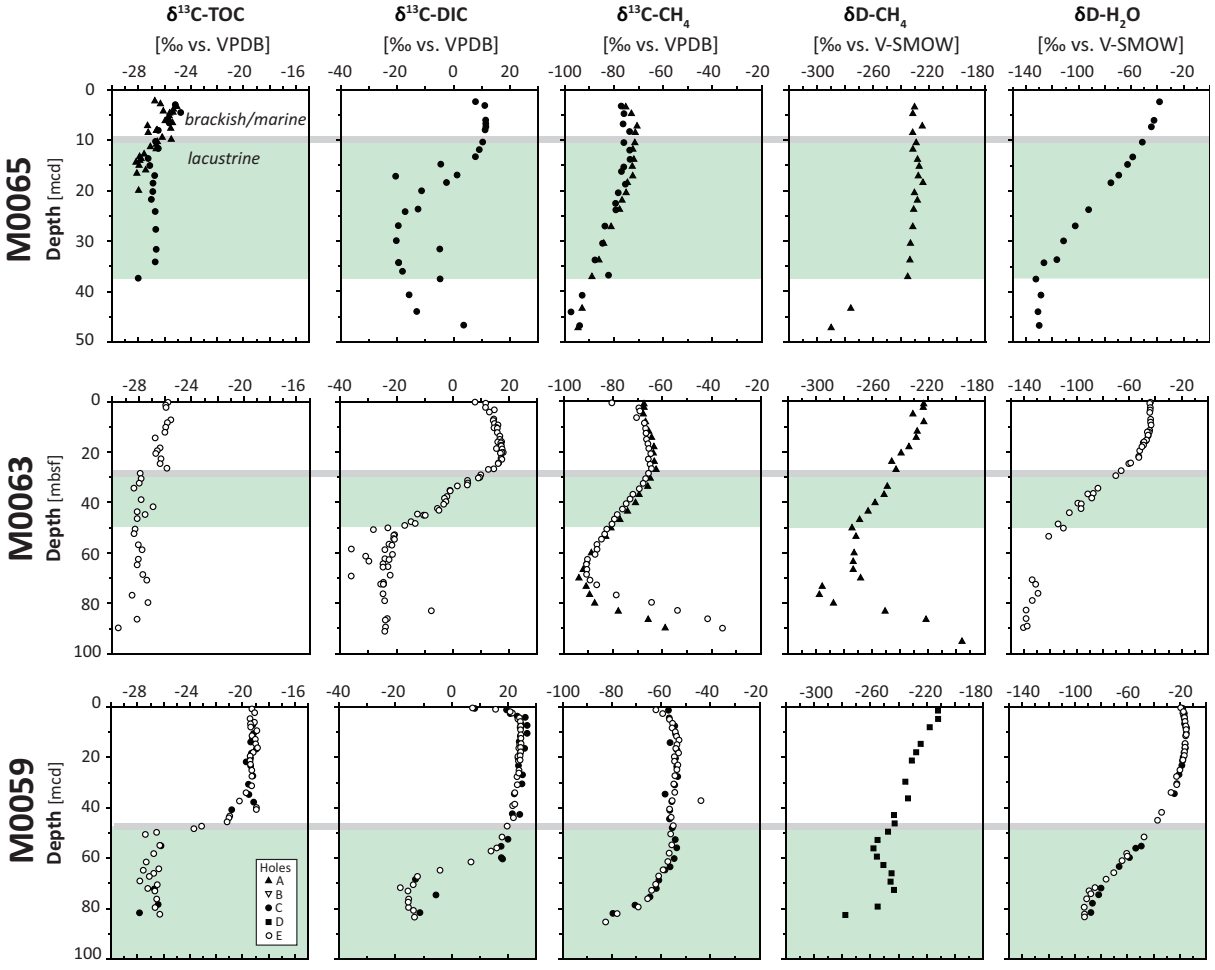

Fig. 6. Isotopic composition of TOC, DIC, CH_4 and H_2O. VPDB = Vienna Pee Dee Belemnite and V-SMOW = Vienna Standard mean ocean water. The gray bar and the green shaded area are explained in the legend of Fig. 3. Note the different depth scale for Site M0065. (For interpretation of the references to colour in this figure legend, the reader is referred to the web version of this article.)

4.3. Fe-stimulated SO_4-AOM via a cryptic S cycle

The presence of pore water SO_4^{2-} and the shifts in $\delta^{13}C$-CH_4 and δD-CH_4 towards isotopically enriched CH_4 suggest that SO_4-AOM is occurring below 70 m depth at Site M0063. The estimated fractionation factor for carbon (ε_C) of ~18‰ ($R^2 = 0.972$) in these sediments is within the range of reported values for SO_4-AOM in marine sediments (~4–30‰) (Whiticar, 1999), while the calculated fractionation factor for hydrogen (ε_H) of ~50‰ ($R^2 = 0.997$) is lower than previously documented values (~95–285‰) (Whiticar, 1999) likely due to the presence of old D-depleted glacial water in the deep limnic clay. It is important to note, however, that these estimated kinetic isotope fractionation factors are derived using the Rayleigh distillation function, which only applies to closed systems (Rayleigh, 1896; Whiticar, 1999). Thus, they should be seen as a first approximation since more accurate estimates would require isotope modeling taking into account diffusive mixing of CH_4 (e.g. Alperin et al., 1988).

Previous studies suggested that the elevated concentrations of pore water SO_4^{2-} at depth in limnic Baltic Sea deposits (Arkona Basin) are a remnant of seawater ions that diffused into the freshwater deposits during the early A/L transgression (Mogollón et al., 2012; Holmkvist et al., 2014). However, these studies focused on the upper <10 m of sediment only. The pore water profile of Cl^- (Fig. 7) and our transient model results both suggest that the increase in dissolved SO_4^{2-} below 70 m depth at Site M0063 is unlikely to be of remnant origin, indicating a possible lateral source of SO_4^{2-}.

SO_4-AOM does not necessarily have to be restricted to the deep sediments with elevated pore water SO_4^{2-} concentrations, as the presence of Fe(III) could cause a recycling of sulfide to SO_4^{2-} in a cryptic sulfur cycle (Holmkvist et al., 2011a):

$$17H_2S + 8FeOOH \rightarrow SO_4^{2-} + 8FeS_2 + 8H_2 + 12H_2O + 2H^+ \quad (V)$$

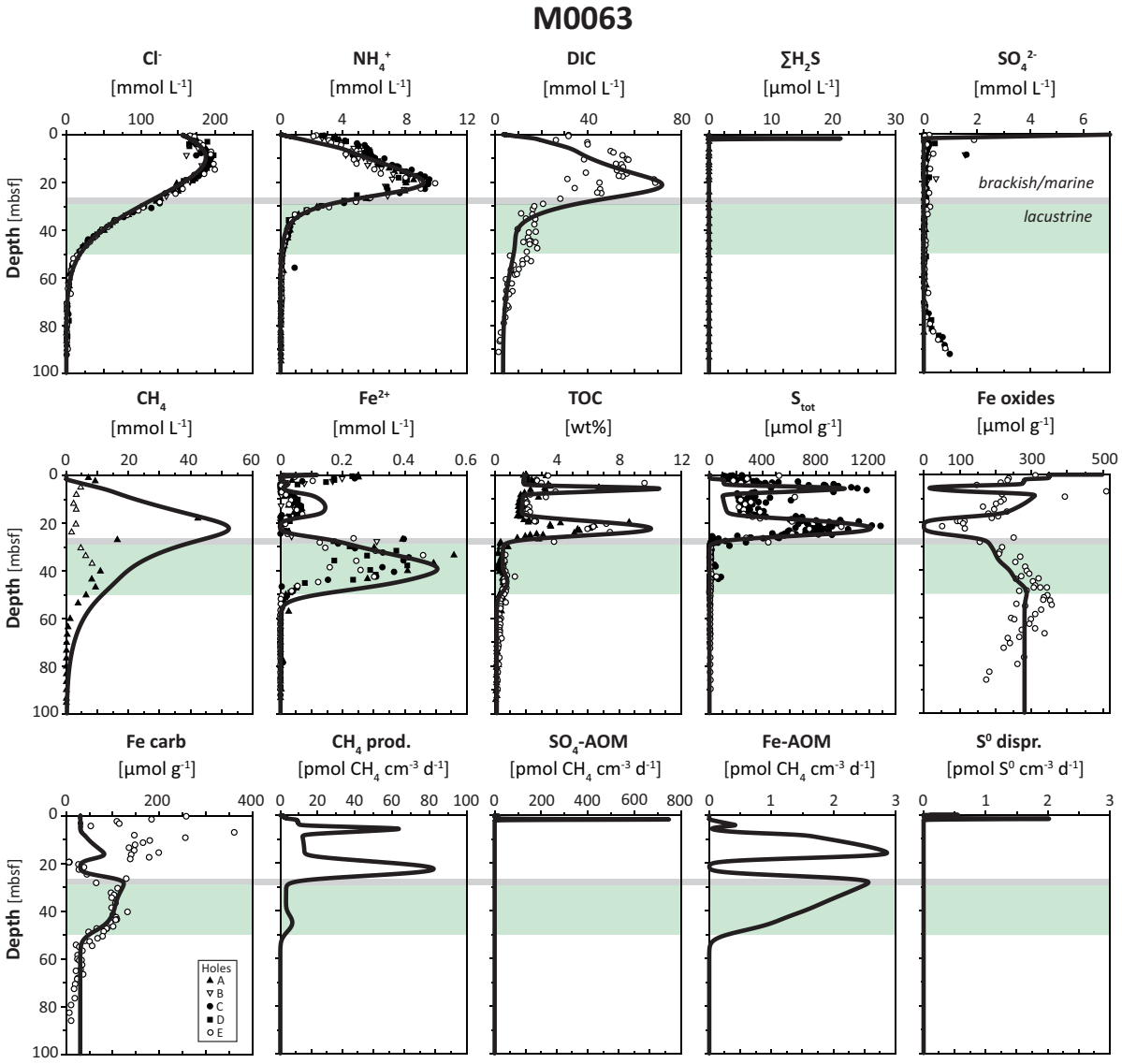

Fig. 7. Site M0063: Pore water and solid phase profiles derived from the diagenetic model (black lines), as well as modeled rates of methanogenesis, SO_4-AOM, Fe-AOM and S^0 disproportionation. The gray bar and the green shaded area are explained in the legend of Fig. 3. The white symbols for CH_4 indicate that these measurements represent the remains of CH_4 after most CH_4 has been lost due to outgassing during coring. (For interpretation of the references to colour in this figure legend, the reader is referred to the web version of this article.)

and thereby fuel SO_4^{2-}-driven AOM in the SO_4^{2-}-depleted limnic deposits. Methanogenic sediments in which a cryptic sulfur cycle was postulated to occur are generally characterized by low background SO_4^{2-} concentrations (<0.5 mM) and low rates of SO_4^{2-} reduction (<1 nmol cm^{-3} d^{-1}) (Leloup et al., 2007, 2009; Knab et al., 2009; Holmkvist et al., 2011a, 2011b; Treude et al., 2014; Brunner et al., 2016; Egger et al., 2016a). Pore water SO_4^{2-} concentrations in the methanogenic sediments rich in dissolved Fe^{2+} observed at Site M0065 are <100 µM and <200 µM for Sites M0063 and M0059, respectively. These values suggest that a cryptic S cycling may be active in deep Baltic Sea sediments.

Such a cryptic S cycle requires the formation of SO_4^{2-} to maintain low rates of SO_4^{2-} reduction. In our diagenetic model for Site M0063, S^0 disproportionation provides the only source of pore water SO_4^{2-} (R16 in Table 2). Formation of S^0, in turn, occurs exclusively through the reaction between dissolved sulfide and reactive Fe(III) (R12 and R13 in Table 2) (Pyzik and Sommer, 1981; Burdige and Nealson, 1986). Pore water sulfide, however, is restricted to the upper 3 m of sediment in the model due to removal by Fe sulfide minerals (Fig. 7). Sensitivity analyses of the key rate constants involved in the modeled cryptic S cycle (Supplementary Figs. S2–S4) and the absence of detectable dissolved sulfide at all three sites (Fig. 5) both indicate that,

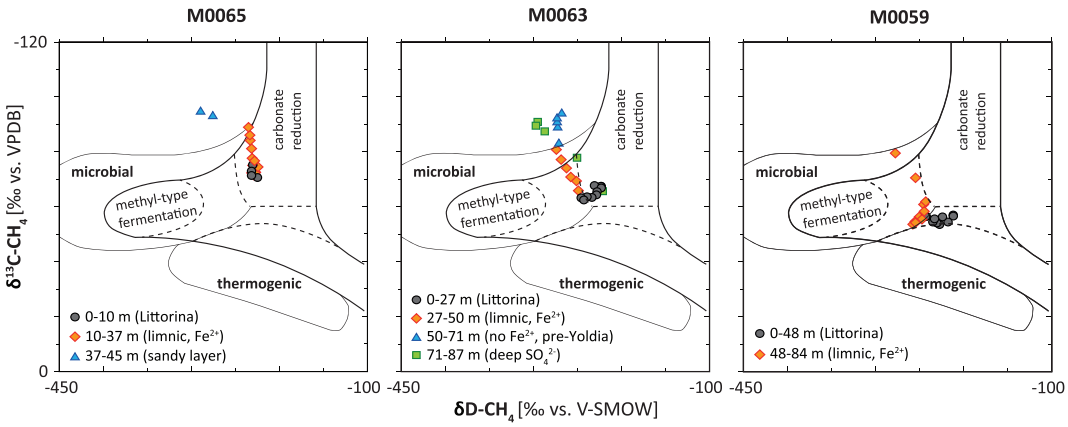

Fig. 8. Methane isotope classification diagram modified after (Whiticar, 1999). Black dots represent samples from Littorina Sea sediments, while red diamonds show samples from the Fe^{2+}-rich sediments below the A/L transition. Blue triangles indicate limnic sediments without dissolved Fe^{2+} and green squares (Site M0063 only) are for samples from deep limnic sediments with elevated pore water SO_4^{2-}. Note that methyl-type fermentation is typically the dominant CH_4 production pathway in freshwater systems, while marine systems are dominated by carbonate reduction. VPDB = Vienna Pee Dee Belemnite and V-SMOW = Vienna Standard mean ocean water. (For interpretation of the references to colour in this figure legend, the reader is referred to the web version of this article.)

if a cryptic S cycle is occurring, a mechanism other than oxidation of dissolved sulfide should be responsible for the low background SO_4^{2-} observed below the A/L transition.

A possible source of SO_4^{2-} not included in our model could be re-oxidation of iron sulfide minerals to S^0 or thiosulfate with sedimentary Fe(III) and subsequent disproportionation (Holmkvist et al., 2011b). Average concentrations of Fe sulfide minerals below the A/L transition of ~30 μmol g^{-1} at Site M0065 (~2% AVS, ~98% CRS), ~11 μmol g^{-1} at Site M0063 (~15% AVS, ~85% CRS) and ~37 μmol g^{-1} at Site M0059 (~4% AVS, ~96% CRS) are generally low and dominated by pyrite (Supplementary Fig. S5), and could theoretically allow for oxidation of Fe sulfides with Fe oxide minerals, e.g. (Aller and Rude, 1988):

$$8FeOOH + FeS + 16H^+ \rightarrow 9Fe^{2+} + SO_4^{2-} + 12H_2O \quad (VI)$$

Although such reactions have been documented at low pH in nonmarine environments, there is only limited evidence for Fe(III) driven re-oxidation of Fe sulfides in laboratory experiments with natural marine sediments (Aller and Rude, 1988; Schippers and Jørgensen, 2002). As a consequence, the reaction between sedimentary Fe(III) and Fe sulfides is currently considered unlikely in natural sediments (Rickard and Luther, 2007). It should be noted, however, that such a reaction could be a slow process, which may not be captured in short-term laboratory incubation experiments. Furthermore, low concentrations of dissolved sulfide, could shift the chemical equilibrium between pore water sulfide and Fe sulfide minerals, resulting in slow dissolution of the latter, a process that is not included in our diagenetic model.

An additional pathway for SO_4^{2-} production is dissolution of sedimentary barite ($BaSO_4$) (Treude et al., 2014). Barite is typically undersaturated in SO_4^{2-}-depleted sediments (e.g. Torres et al., 1996; Riedinger et al., 2006; Henkel et al., 2012) and has been shown to be a potential source of SO_4^{2-} for SO_4^{2-} reducing bacteria (Karnachuk et al., 2002). Elevated concentrations of pore water Ba^{2+} in the Fe^{2+}-rich sediments at all sites of up to ~30 μM (Andrén et al., 2015) indicate that $BaSO_4$ dissolution below the A/L transition could indeed facilitate slow rates of SO_4^{2-} reduction in these sediments.

Finally, the low concentrations of pore water SO_4^{2-} in the deep sediments could also be the result of an artifact caused by contamination with seawater SO_4^{2-}. As recently demonstrated for sediments from Aarhus Bay, a contamination with only a few μL of seawater would be sufficient to result in the apparent SO_4^{2-} concentrations of 100–200 μM observed in the methanogenic sediments here (Brunner et al., 2016). Nevertheless, if occurring, continuous production of sulfide through low rates of SO_4^{2-} reduction could result in a net accumulation of pore water Fe^{2+} by reactions between sulfide and sedimentary Fe oxides, provided that the latter reaction is faster than authigenic FeS formation with dissolved Fe^{2+} or that it occurs in microenvironments. The high reactivity of dissolved sulfide towards Fe^{2+} (Berner and Westrich, 1985; Rickard and Luther, 2007) and our model sensitivity analyses (Supplementary Figs. S2–S4), however, indicate that released sulfide would be immediately scavenged by Fe^{2+} to form Fe sulfides. Thus, such a potential cryptic S cycle is unlikely to result in significant accumulation of pore water Fe^{2+} (e.g. Egger et al., 2016a).

4.4. Fe-AOM below the A/L transition

Downward diffusion of CH_4 into the limnic clay, which is dominated by low concentrations of refractory organic matter, indicates that CH_4 may provide a potential reductant for the sedimentary Fe oxides. To test whether Fe-AOM can produce the high concentrations of Fe^{2+} below the A/L transition at Site M0063, we assumed in the diagenetic model that Fe oxides buried past the initial zone of

organoclastic Fe reduction are not available for organoclastic Fe reducers. Thus, organoclastic Fe reduction is limited to the upper ~20 cm sediment depth in the model (Supplementary Fig. S1). Fe-AOM therefore represents the only Fe oxide reduction pathway at depth in the model. As a consequence of this assumption, the model results cannot be interpreted as proof for Fe-AOM but rather are used to assess whether it is a possible mechanism.

The model shows that assuming Fe-AOM as the only Fe reduction pathway enables a good fit between the modeled and measured pore water and solid phase profiles (Fig. 7). Model-derived rates for Fe-AOM of up ~3 pmol CH_4 cm^{-3} d^{-1} are in between potential Fe-AOM rates from stimulated laboratory incubation studies (~4 nmol CH_4 cm^{-3} d^{-1}) (Sivan et al., 2011; Segarra et al., 2013; Egger et al., 2015b) and recently estimated potential Fe-AOM rates in deep Black Sea sediments (~0.04 pmol CH_4 cm^{-3} d^{-1}) (Egger et al., 2016a). Depth-integrated rates of SO_4-AOM (~240 μmol CH_4 m^{-2} d^{-1}) and Fe-AOM (~68 μmol CH_4 m^{-2} d^{-1}) over the whole model domain (i.e. 0–100 m depth) indicate that Fe-AOM could account for ~20% of total anaerobic CH_4 oxidation in the sediments at Site M0063. Note that this estimate is based on the assumption that Fe-AOM is responsible for all of the Fe reduction at depth in the sediment. Hence, it should be seen as a theoretical upper estimate. However, the model shows that although rates of SO_4-AOM are much higher than those of Fe-AOM (~740 pmol CH_4 cm^{-3} d^{-1} vs. ~2.5 pmol CH_4 cm^{-3} d^{-1}), CH_4 consumption through Fe-AOM could still be significant as it occurs over a much greater depth interval. The model further suggests that a major sink for CH_4 produced in the Littorina Sea sediments is downward transport into the lake deposits (~406 μmol CH_4 m^{-2} d^{-1}, of which ~191 μmol CH_4 m^{-2} d^{-1} is diffusive and ~215 μmol CH_4 m^{-2} d^{-1} is advective, i.e. due to burial). In addition, the modeled depth-integrated rate of Fe-AOM for the limnic deposits (~37 μmol CH_4 m^{-2} d^{-1}) reveals that removal of <10% of the downward transported, Littorina Sea-derived CH_4 through Fe-AOM would be sufficient to explain the elevated concentrations of Fe^{2+} in the pore water below the A/L transition at Site M0063, due to the 8:1 Fe-CH_4 stoichiometry of Fe-AOM.

Preferential oxidation of isotopically light CH_4 during AOM results in a progressive enrichment of the residual pore water CH_4 in ^{13}C-CH_4 and D-CH_4 (Alperin et al., 1988; Martens et al., 1999; Reeburgh, 2007). The observed depletions in ^{13}C-CH_4 and D-CH_4 of pore water CH_4 below the A/L transition, however, are the opposite of what is expected if CH_4 concentrations are controlled exclusively by oxidation of downward diffusing Littorina Sea-derived CH_4 through Fe-AOM (Fig. 6). Previous studies have shown that in systems where production and oxidation of CH_4 take place concurrently, generation of ^{13}C-depleted CH_4 during methanogenesis may conceal the isotopic signature of AOM (Borowski et al., 1997; Seifert et al., 2006; Egger et al., 2015b). Thus, the continuous depletion in ^{13}C of the pore water CH_4 with decreasing CH_4 concentrations below the A/L transition could be the result of CH_4 production from strongly ^{13}C-depleted DIC in the limnic deposits (Fig. 6). It is interesting to note that at Site M0065, the $\delta^{13}C$-CH_4 signal shows almost no change with sediment depth down to ~15 m followed by a depletion in ^{13}C (Fig. 6). Based on the discussion in Section 4.2, this observation may indicate lower rates of methanogenesis due to the relatively high amounts of amorphous Fe oxides in the sediments between the A/L transition and ~15 m depth (Fig. 3) when compared to the sediments below 15 m depth, and a higher contribution of the isotopic signature of CH_4 consumption potentially through Fe-AOM.

In addition, the higher diffusivity of the lighter $^{12}CH_4$ molecules compared to the heavier $^{13}CH_4$ molecules further results in a negative isotope fractionation (~3–5‰) of the downward diffusing CH_4 (Happell et al., 1995; Chanton, 2005; Xia and Tang, 2012). Thus, in non-steady state systems as the one considered here, passive downward diffusion may add to the observed depletion in ^{13}C of the pore water CH_4 and hence further obscure a potential isotopic signature of Fe-AOM. Note that the upwards and downwards diffusion loss of isotopically light CH_4 out of the Littorina Sea sediments also causes a preferential ^{12}C depletion in DIC, contributing to the heavy $\delta^{13}C$-DIC observed in these sediments (Fig. 6).

Another explanation for the shift to ^{13}C-depleted CH_4 below the A/L transition is enzyme-mediated equilibrium carbon isotope exchange during AOM (Holler et al., 2012; Yoshinaga et al., 2014). Such a microbially mediated C isotope equilibration between CH_4 and CO_2 is most pronounced when the reaction takes place close to thermodynamic equilibrium (Holler et al., 2012; Yoshinaga et al., 2014). Yoshinaga et al. (2014) showed that SO_4-AOM at low SO_4^{2-} concentrations (<0.5 mM) might, in fact, result in ^{13}C-depletion in the CH_4 rather than ^{13}C-enrichment as generally observed by CH_4 oxidation. The authors attributed the ^{13}C-depletion of CH_4 to an enzyme-level reversibility leading to an apparent inverse isotope effect, where the relative equilibrium fractionation of the reverse reaction (i.e. AOM back flux) is larger than that of the forward reaction at low SO_4^{2-} concentrations. Considering the slow rates reported for Fe-AOM (Beal et al., 2009; Sivan et al., 2011; Segarra et al., 2013; Egger et al., 2015b, 2016a) and the low accessibility of Fe oxides in comparison to dissolved SO_4^{2-}, Fe-AOM is likely to operate close to thermodynamic equilibrium, thereby potentially enabling equilibrium isotope exchange. Such an enzyme-mediated equilibrium carbon isotope exchange should, in theory, also result in ^{13}C-enriched DIC. The shift in $\delta^{13}C$-DIC towards more depleted values in the Fe^{2+}-rich sediments below the A/L transition, as observed at all three sites (Fig. 6), shows that this mechanism is unlikely to explain all of the ^{13}C-depletion in CH_4 with depth.

More ^{13}C-depleted DIC below the A/L transition, on the other hand, is consistent with the preferential oxidation of ^{12}C-CH_4 during Fe-AOM and the subsequent addition of isotopically light ^{12}C-CO_2 to the DIC pool. Due to the slow rates of Fe-AOM, however, such a negative excursion in $\delta^{13}C$-DIC is likely to mainly derive from the lower rates of methanogenesis below the A/L transition (see also Fig. 7) and thus less removal of isotopically light CO_2 from the DIC pool, as well as more ^{13}C-depleted organic matter

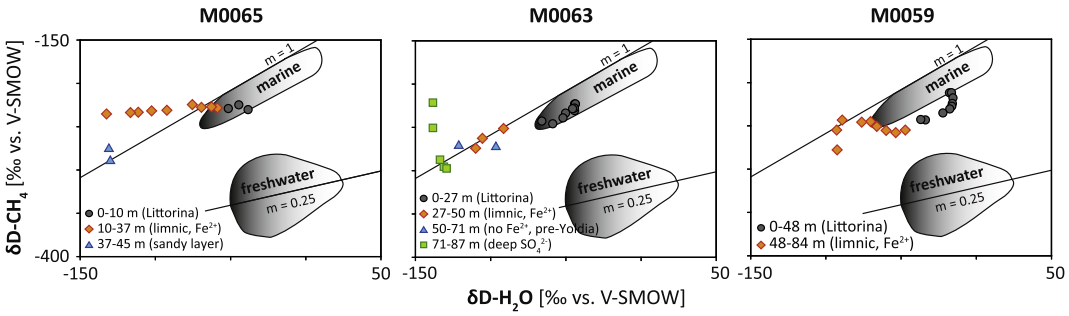

Fig. 9. Dependence of hydrogen isotope ratio in methane (δD-CH_4) as a function of the hydrogen isotope ratio of the coexisting pore water (δD-H_2O), modified after (Whiticar, 1999). Methanogenesis by carbonate reduction (the dominant CH_4 pathway in marine systems) follows a slope "m" of 1, while the methyl-type fermentation pathway (the dominant CH_4 pathway in freshwater systems) has a slope "m" of ~0.25. Gray shaded area indicate values reported by (Whiticar, 1999). Black dots represent samples from Littorina Sea sediments, while red diamonds show samples from the Fe^{2+}-rich sediments below the A/L transition. Blue triangles indicate limnic sediments without dissolved Fe^{2+} and green squares (Site M0063 only) are from deep limnic sediments with elevated pore water SO_4^{2-}. V-SMOW = Vienna Standard mean ocean water. (For interpretation of the references to colour in this figure legend, the reader is referred to the web version of this article.)

in the deep limnic deposits when compared to the Littorina Sea sediments (Fig. 6).

For hydrogenotrophic carbonate reduction, the pore water represents the initial hydrogen source for the formation of CH_4 (Daniels et al., 1980; Whiticar, 1999). The dependence of δD-CH_4 on the hydrogen isotope ratio of the coexisting pore water (δD-H_2O) in Littorina Sea sediments falls within the range typically observed for marine methanogenesis by carbonate reduction (Fig. 9). However, CH_4 in the Fe^{2+}-rich sediments below the A/L transition appears to be enriched in D compared to what would be expected from the ambient pore water at all sites. This relative enrichment in D-CH_4 compared to D-H_2O is especially pronounced at Site M0065 and M0059 and is likely due to mixing with downward diffusing Littorina Sea-derived CH_4 enriched in D (Fig. 6). Interestingly, the limnic deposits below the zones of high dissolved Fe^{2+} show an abrupt change towards lighter δD-CH_4 at Site M0065 consistent with hydrogenotrophic CH_4 production with coexisting pore water. Such a sharp transition may indicate a lack of addition of D-enriched CH_4 by the absence of Fe-AOM below the Fe^{2+}-rich deposits, which would also be consistent with an increase in δ^{13}C-DIC (i.e. less addition of ^{12}C-CO_2 from Fe-AOM) observed in these sediments (Fig. 6). A similar change towards lighter δD-CH_4 is observed at the bottom of the core at Site M0059. However, pore water concentrations of Fe^{2+} appear to remain high in these sediments. Note that the D-enriched CH_4 below 70 m depth at Site M0063 is likely due to SO_4-AOM with pore water SO_4^{2-} present at depth (as discussed in Section 4.3).

In summary, the good correlation between pore water Fe^{2+} and the presence of CH_4 in the limnic clay at all three sites (Fig. 5) suggests a potential coupling between CH_4 oxidation and Fe oxide reduction below the A/L transition. While methanogenesis dominates the profiles of δ^{13}C-CH_4 and δ^{13}C-DIC, δD-CH_4 may indicate D-enrichment in pore water CH_4 due to Fe-AOM. However, the addition of D-enriched Littorina Sea-derived CH_4 complicates the interpretation of the relative enrichment in δD-CH_4 compared to ambient δD-H_2O. Thus, although geochemical evidence points towards Fe-mediated CH_4 oxidation in deep Baltic Sea sediments, the concurrent production, consumption and transport of CH_4 make it difficult to conclusively assess whether Fe-AOM is occurring in these sediments based on geochemical profiles. The diagenetic model developed for Site M0063 shows that the pore water and solid phase profiles can be reproduced with Fe-AOM as a Fe reduction pathway in the deep Baltic Sea sediments. Due to the underlying model assumptions, however, the model results cannot be interpreted as proof for Fe-AOM. Hence, additional laboratory incubation studies of these sediments are needed to confirm that the in-situ microbial community is capable of linking CH_4 oxidation to Fe oxide reduction.

5. CONCLUSIONS

In the Baltic Sea, the transition from the Ancylus freshwater phase to the Littorina brackish/marine phase at 9–7 kyr BP resulted in the accumulation of organic-rich methanogenic sediments overlying organic-poor limnic deposits. The present downward diffusion of CH_4 from the Littorina Sea sediments into the Fe oxide-rich lake deposits may enable a coupling between Fe oxide reduction and CH_4 oxidation (Fe-AOM). Our results reveal a complex interplay between production, oxidation and downward diffusion of dissolved CH_4 in deep Baltic Sea sediments. We propose that removal of a small part (~10%) of the downward transported CH_4 through Fe-AOM within the Fe oxide-rich lake deposits would be sufficient to explain the elevated concentrations of Fe^{2+} in the pore water below the A/L transition, due to the 8:1 Fe-CH_4 stoichiometry of the reaction. The findings in this study support recent evidence that CH_4 represents a plausible electron donor for the reduction of more crystalline Fe oxides in SO_4^{2-}-depleted and organic-poor environments (Riedinger et al., 2014; Egger et al., 2016a; Sivan et al., 2016), likely through a direct electron transfer between methanotrophic archaea and Fe oxides (McGlynn et al., 2015; Wegener et al., 2015; Scheller et al., 2016). Our results

show that changes in bottom water salinity due to post-glacial global sea-level rise could result in the reduction of deeply buried Fe oxides with pore water CH_4 in former lake deposits thus impacting sedimentary Fe cycling and related biogeochemical processes, such as burial of phosphorus (Dijkstra et al., 2016; Egger et al., 2016a).

ACKNOWLEDGMENTS

We thank the captain, crew and shipboard party of the IODP Expedition 347 aboard Greatship Manisha in 2013. T. Zalm, D. van de Meent, T. Claessen, M. van Erk, A. van Dijk, I. Schmiedinger, J. Pedersen, K. Bomholt Oest, I. Stimac, M. Lutiker and C. Carter are acknowledged for invaluable technical and analytical support. This research was funded by the European Research Council under the European Community's Seventh Framework Program (ERC Starting Grant #278364 to C. P. S.), the Netherlands Organization for Scientific Research (NWO-Vici Grant 865.13.005), the Consortium for Ocean Leadership – U.S. Science Support Program (NR) and the Integrated Ocean Drilling Program (IODP). Hydrogen isotope measurements on interstitial water samples were supported by the Leibniz Association (IOW). We further acknowledge financial support from ERC Advanced Grant #294200 to B. B. J. and from the Helmholtz Association (Alfred Wegener Institute Helmholtz Centre for Polar and Marine Research). This work was carried out under the program of the Netherlands Earth System Science Center (NESSC), financially supported by the Ministry of Education, Culture and Science (OCW).

APPENDIX A. SUPPLEMENTARY MATERIAL

Supplementary data associated with this article can be found, in the online version, at http://dx.doi.org/10.1016/j.gca.2017.03.019.

REFERENCES

Achtnich C., Bak F. and Conrad R. (1995) Competition for electron donors among nitrate reducers, ferric iron reducers, sulfate reducers, and methanogens in anoxic paddy soil. *Biol. Fertil. Soils* **19**, 65–72.

Aller R. C. and Rude P. D. (1988) Complete oxidation of solid phase sulfides by manganese and bacteria in anoxic marine sediments. *Geochim. Cosmochim. Acta* **52**, 751–765.

Alperin M. J., Reeburgh W. S. and Whiticar M. J. (1988) Carbon and hydrogen isotope fractionation resulting from anaerobic methane oxidation. *Glob. Biogeochem. Cycl.* **2**, 279–288.

Amos R. T., Bekins B. A., Cozzarelli I. M., Voytek M. A., Kirshtein J. D., Jones E. J. P. and Blowes D. W. (2012) Evidence for iron-mediated anaerobic methane oxidation in a crude oil-contaminated aquifer. *Geobiology* **10**, 506–517.

Andrén E., Andrén T. and Sohlenius G. (2000) The Holocene history of the southwestern Baltic Sea as reflected in a sediment core from the Bornholm Basin. *Boreas* **29**, 233–250.

Andrén T., Jørgensen B. B., Cotterill C., G S., and the Expedition 347 Scientists (2015). Integrated ocean drilling program. In: Proceedings of IODP, College Station, TX, p. 347.

Arndt S., Brumsack H.-J. and Wirtz K. W. (2006) Cretaceous black shales as active bioreactors: a biogeochemical model for the deep biosphere encountered during ODP Leg 207 (Demerara Rise). *Geochim. Cosmochim. Acta* **70**, 408–425.

Beal E. J., House C. H. and Orphan V. J. (2009). Manganese- and iron-dependent marine methane oxidation. Science 325(80-.), 184–187.

Berg P., Rysgaard S. and Thamdrup B. (2003) Dynamic modeling of early diagenesis and nutrient cycling. A case study in an Arctic marine sediment. *Am. J. Sci.* **303**, 905–955.

Berner R. A. and Westrich J. T. (1985) Bioturbation and the early diagenesis of carbon and sulfur. *Am. J. Sci.* **285**, 193–206.

Bethke C. M., Sanford R. A., Kirk M. F., Jin Q. and Flynn T. M. (2011) The thermodynamic ladder in geomicrobiology. *Am. J. Sci.* **311**, 183–210.

Björck S. (1995) A review of the history of the Baltic Sea, 13.0–8.0 ka BP. *Quat. Int.* **27**, 19–40.

Bodegom P. M., Scholten J. C. M. and Stams A. J. M. (2004) Direct inhibition of methanogenesis by ferric iron. *FEMS Microbiol. Ecol.* **49**, 261–268.

Boesen C. and Postma D. (1988) Pyrite formation in anoxic environments of the Baltic. *Am. J. Sci.* **288**, 575–603.

Boetius A., Ravenschlag K., Schubert C. J., Rickert D., Widdel F., Gieseke A., Amann R., Jørgensen B. B., Witte U. and Pfannkuche O. (2000) A marine microbial consortium apparently mediating anaerobic oxidation of methane. *Nature* **407**, 623–626.

Bond D. R. and Lovley D. R. (2002) Reduction of Fe(III) oxide by methanogens in the presence and absence of extracellular quinones. *Environ. Microbiol.* **4**, 115–124.

Borowski W. S., Paull C. K. and Ussier W. (1997) Carbon cycling within the upper methanogenic zone of continental rise sediments: an example from the methane-rich sediments overlying the blake ridge gas hydrate deposits. *Mar. Chem.* **57**, 299–311.

Böttcher M. E. and Lepland A. (2000) Biogeochemistry of sulfur in a sediment core from the west-central Baltic Sea: evidence from stable isotopes and pyrite textures. *J. Mar. Syst.* **25**, 299–312.

Boudreau B. P. (1996) The diffusive tortuosity of fine-grained unlithified sediments. *Geochim. Cosmochim. Acta* **60**, 3139–3142.

Boudreau B. P. (1997) *Diagenetic Models and Their Implementation. Modelling Transport and Reactions in Aquatic Sediments*. Springer.

Brass M. and Röckmann T. (2010) Continuous-flow isotope ratio mass spectrometry method for carbon and hydrogen isotope measurements on atmospheric methane. *Atmos. Meas. Tech.* **3**, 1707–1721.

Brunner B., Arnold G. L., Røy H., Müller I. A. and Jørgensen B. B. (2016) Off limits: sulfate below the sulfate-methane transition. *Front. Earth Sci.* **4**, 1–16.

Burdige D. J. and Nealson K. H. (1986) Chemical and microbiological studies of sulfide-mediated manganese reduction. *Geomicrobiol. J.* **4**, 361–387.

Burton E. D., Sullivan L. A., Bush R. T., Johnston S. G. and Keene A. F. (2008) A simple and inexpensive chromium-reducible sulfur method for acid-sulfate soils. *Appl. Geochem.* **23**, 2759–2766.

Chanton J. P. (2005) The effect of gas transport on the isotope signature of methane in wetlands. *Org. Geochem.* **36**, 753–768.

Coplen T. B., Brand W. A., Gehre M., Gröning M., Meijer H. A. J., Toman B. and Verkouteren R. M. (2006) New guidelines for δ13C measurements. *Anal. Chem.* **78**, 2439–2441.

Crowe S. A., Katsev S., Leslie K., Sturm A., Magen C., Nomosatryo S., Pack M. A., Kessler J. D., Reeburgh W. S., Roberts J. A., González L., Douglas Haffner G., Mucci A., Sundby B. and Fowle D. A. (2011) The methane cycle in ferruginous Lake Matano. *Geobiology* **9**, 61–78.

Cruz Viggi C., Rossetti S., Fazi S., Paiano P., Majone M. and Aulenta F. (2014) Magnetite particles triggering a faster and

more robust syntrophic pathway of methanogenic propionate degradation. *Environ. Sci. Technol.* **48**, 7536–7543.

Daniels L., Fulton G., Spencer R. W. and Orme-Johnson W. H. (1980) Origin of hydrogen in methane produced by Methanobacterium thermoautotrophicum. *J. Bacteriol.* **141**, 694–698.

Dijkstra N., Slomp C. P. and Behrends T.Expedition 347 Scientists (2016) Vivianite is a key sink for phosphorus in sediments of the Landsort Deep, an intermittently anoxic deep basin in the Baltic Sea. *Chem. Geol.* **438**, 58–72.

Egger M., Jilbert T., Behrends T., Rivard C. and Slomp C. P. (2015a) Vivianite is a major sink for phosphorus in methanogenic coastal surface sediments. *Geochim. Cosmochim. Acta* **169**, 217–235.

Egger M., Kraal P., Jilbert T., Sulu-Gambari F., Sapart C. J., Röckmann T. and Slomp C. P. (2016a) Anaerobic oxidation of methane alters sediment records of sulfur, iron and phosphorus in the Black Sea. *Biogeosciences* **13**, 5333–5355.

Egger M., Lenstra W., Jong D., Meysman F. J. R., Sapart C. J., van der Veen C., Röckmann T., Gonzalez S. and Slomp C. P. (2016b) Rapid sediment accumulation results in high methane effluxes from coastal sediments. *PLoS One* **11**, e0161609.

Egger M., Rasigraf O., Sapart C. J., Jilbert T., Jetten M. S. M., Röckmann T., van der Veen C., Bândă N., Kartal B., Ettwig K. F. and Slomp C. P. (2015b) Iron-mediated anaerobic oxidation of methane in brackish coastal sediments. *Environ. Sci. Technol.* **49**, 277–283.

Ettwig K. F., Zhu B., Speth D., Keltjens J. T., Jetten M. S. M. and Kartal B. (2016) Archaea catalyze iron-dependent anaerobic oxidation of methane. *Proc. Natl. Acad. Sci.* **113**, 12792–12796.

Froelich P. N., Klinkhammer G. P., Bender M. L., Luedtke N. A., Heath G. R., Cullen D., Dauphin P., Hammond D., Hartman B. and Maynard V. (1979) Early oxidation of organic matter in pelagic sediments of the eastern equatorial Atlantic: suboxic diagenesis. *Geochim. Cosmochim. Acta* **43**, 1075–1090.

Happell J. J. D., Chanton J. P. J. and Showers W. W. J. (1995) Methane transfer across the water-air interface in stagnant wooded swamps of Florida: evaluation of mass-transfer coefficients and isotopic fractionation. *Limnol. Oceanogr.* **40**, 290–298.

Henkel S., Mogollón J. M., Nöthen K., Franke C., Bogus K., Robin E., Bahr A., Blumenberg M., Pape T., Seifert R., März C., de Lange G. J. and Kasten S. (2012) Diagenetic barium cycling in Black Sea sediments - a case study for anoxic marine environments. *Geochim. Cosmochim. Acta* **88**, 88–105.

Hindmarsh A. C. (1983). ODEPACK, a systematized collection of ODE solvers. In: Stepleman R. S., et al. (Eds.), IMACS Transactions on Scientific Computation, vol. 1. North-Holland, Amsterdam, pp. 55–64.

Hinrichs K. U., Hayes J. M., Sylva S. P., Brewer P. G. and DeLong E. F. (1999) Methane-consuming archaebacteria in marine sediments. *Nature* **398**, 802–805.

Hoehler T. M., Alperin M. J., Albert D. B. and Martens C. S. (1994) Field and laboratory studies of methane oxidation in an anoxic marine sediment: Evidence for a methanogen-sulfate reducer consortium. *Global Biogeochem. Cycles* **8**, 451–463.

Holler T., Wegener G., Niemann H., Ferdelman T. G., Boetius A., Kristiansen T. Z., Molina H., Pandey A., Werner J. K., Juluri K. R., Xu Y., Glenn D., Parang K. and Snyder S. H. (2012) Carbon and sulfur back flux during anaerobic microbial oxidation of methane and coupled sulfate reduction. *Proc. Natl. Acad. Sci.* **109**, 21170–21170.

Holmkvist L., Ferdelman T. G. and Jørgensen B. B. (2011) A cryptic sulfur cycle driven by iron in the methane zone of marine sediment (Aarhus Bay, Denmark). *Geochim. Cosmochim. Acta* **75**, 3581–3599.

Holmkvist L., Kamyshny A., Brüchert V., Ferdelman T. G. and Jørgensen B. B. (2014) Sulfidization of lacustrine glacial clay upon Holocene marine transgression (Arkona Basin, Baltic Sea). *Geochim. Cosmochim. Acta* **142**, 75–94.

Holmkvist L., Kamyshny A., Vogt C., Vamvakopoulos K., Ferdelman T. G. and Jørgensen B. B. (2011) Sulfate reduction below the sulfate–methane transition in Black Sea sediments. *Deep Sea Res. Part I Oceanogr. Res. Pap.* **58**, 493–504.

Hsu T.-W., Jiang W.-T. and Wang Y. (2014) Authigenesis of vivianite as influenced by methane-induced sulfidization in cold-seep sediments off southwestern Taiwan. *J. Asian Earth Sci.* **89**, 88–97.

Jilbert T. and Slomp C. P. (2013) Rapid high-amplitude variability in Baltic Sea hypoxia during the Holocene. *Geology* **41**, 1183–1186.

Jørgensen B. B., Böttcher M. E., Lüschen H., Neretin L. N. and Volkov I. I. (2004) Anaerobic methane oxidation and a deep H2S sink generate isotopically heavy sulfides in Black Sea sediments. *Geochim. Cosmochim. Acta* **68**, 2095–2118.

Karnachuk O., Kurochkina S. and Tuovinen O. (2002) Growth of sulfate-reducing bacteria with solid-phase electron acceptors. *Appl. Microbiol. Biotechnol.* **58**, 482–486.

Kasten S., Freudenthal T., Gingele F. X. and Schulz H. D. (1998) Simultaneous formation of iron-rich layers at different redox boundaries in sediments of the Amazon deep-sea fan. *Geochim. Cosmochim. Acta* **62**, 2253–2264.

Kato S., Hashimoto K. and Watanabe K. (2012) Methanogenesis facilitated by electric syntrophy via (semi)conductive iron-oxide minerals. *Environ. Microbiol.* **14**, 1646–1654.

Knab N. J., Cragg B. A., Hornibrook E. R. C., Holmkvist L., Pancost R. D., Borowski C., Parkes R. J. and Jørgensen B. B. (2009) Regulation of anaerobic methane oxidation in sediments of the Black Sea. *Biogeosciences*, 1505–1518.

Knittel K. and Boetius A. (2009) Anaerobic oxidation of methane: progress with an unknown process. *Annu. Rev. Microbiol.* **63**, 311–334.

Leloup J., Fossing H., Kohls K., Holmkvist L., Borowski C. and Jørgensen B. B. (2009) Sulfate-reducing bacteria in marine sediment (Aarhus Bay, Denmark): abundance and diversity related to geochemical zonation. *Environ. Microbiol.* **11**, 1278–1291.

Leloup J., Loy A., Knab N. J., Borowski C., Wagner M. and Jørgensen B. B. (2007) Diversity and abundance of sulfate-reducing microorganisms in the sulfate and methane zones of a marine sediment, Black Sea. *Environ. Microbiol.* **9**, 131–142.

Lenz C., Jilbert T., Conley D. J. and Slomp C. P. (2015) Hypoxia-driven variations in iron and manganese shuttling in the Baltic Sea over the past 8 kyr. *Geochem. Geophys. Geosyst.* **16**, 3754–3766.

Li H., Chang J., Liu P., Fu L., Ding D. and Lu Y. (2014) Direct interspecies electron transfer accelerates syntrophic oxidation of butyrate in paddy soil enrichments. *Environ. Microbiol.* **17**, 1–45.

Liu D., Wang H., Dong H., Qiu X., Dong X. and Cravotta C. A. (2011) Mineral transformations associated with goethite reduction by Methanosarcina barkeri. *Chem. Geol.* **288**, 53–60.

Lovley D. R. (1991) Dissimilatory Fe(III) and Mn(IV) reduction. *Microbiol. Rev.* **55**, 259–287.

Lovley D. R. and Phillips E. J. P. (1987) Competitive mechanisms for inhibition of sulfate reduction and methane production in the zone of ferric iron reduction in sediments. *Appl. Environ. Microbiol.* **53**.

Lovley D. R., Phillips E. J. P. and Lonergan D. J. (1989) Hydrogen and formate oxidation coupled to dissimilatory reduction of iron or manganese by Alteromonas putrefaciens. *Appl. Environ. Microbiol.* **55**, 700–706.

Mackin J. E. and Aller R. C. (1984) Ammonium adsorption in marine sediments. *Limnol. Oceanogr.* **29**, 250–257.

Martens C. S., Albert D. B. and Alperin M. J. (1999) Stable isotope tracing of anaerobic methane oxidation in the gassy sediments of Eckernforde Bay, German Baltic Sea. *Am. J. Sci.* **299**, 589–610.

März C., Hoffmann J., Bleil U., de Lange G. J. and Kasten S. (2008) Diagenetic changes of magnetic and geochemical signals by anaerobic methane oxidation in sediments of the Zambezi deep-sea fan (SW Indian Ocean). *Mar. Geol.* **255**, 118–130.

McGlynn S. E., Chadwick G. L., Kempes C. P. and Orphan V. J. (2015) Single cell activity reveals direct electron transfer in methanotrophic consortia. *Nature* **526**, 531–535.

Meyerdierks A., Kube M., Kostadinov I., Teeling H., Glöckner F. O., Reinhardt R. and Amann R. (2010) Metagenome and mRNA expression analyses of anaerobic methanotrophic archaea of the ANME-1 group. *Environ. Microbiol.* **12**, 422–439.

Meysman F. J. R., Boudreau B. P. and Middelburg J. J. (2005) Modeling reactive transport in sediments subject to bioturbation and compaction. *Geochim. Cosmochim. Acta* **69**, 3601–3617.

Middelburg J. J. (1991) Organic carbon, sulphur, and iron in recent semi-euxinic sediments of Kau Bay, Indonesia. *Geochim. Cosmochim. Acta* **55**, 815–828.

Milucka J., Ferdelman T. G., Polerecky L., Franzke D., Wegener G., Schmid M., Lieberwirth I., Wagner M., Widdel F. and Kuypers M. M. M. (2012) Zero-valent sulphur is a key intermediate in marine methane oxidation. *Nature* **491**, 541–546.

Mogollón J. M., Dale aW., Fossing H. and Regnier P. (2012) Timescales for the development of methanogenesis and free gas layers in recently-deposited sediments of Arkona Basin (Baltic Sea). *Biogeosciences* **9**, 1915–1933.

Moodley L., Middelburg J. J., Herman P. M. J., Soetaert K. and de Lange G. J. (2005) Oxygenation and organic-matter preservation in marine sediments: direct experimental evidence from ancient organic carbon–rich deposits. *Geology* **33**, 889.

Moran J. J., Beal E. J., Vrentas J. M., Orphan V. J., Freeman K. H. and House C. H. (2008) Methyl sulfides as intermediates in the anaerobic oxidation of methane. *Environ. Microbiol.* **10**, 162–173.

Myhre G., Schindell D., Bréon F. M., Collins W., Fuglestvedt J., Huang J., Koch D., Lamarque J. F., Lee D., Mendoza B., Nakajima T., Robock A., Stephens G., Takemura T. and Zhang H. (2013) Anthropogenic and natural radiative forcing. In *Climate Change 2013: The physical science basis* (eds. T. F. Stocker, D. Qin, G. K. Plattner, M. Tignor, S. K. Allen, J. Boschung, A. Nauels, Y. Xia, V. Bex and P. M. Midgley). Cambridge University Press, Cambridge, United Kingdom and New York, NY, USA.

Neretin L. N., Böttcher M. E., Jørgensen B. B., Volkov I. I., Lüschen H. and Hilgenfeldt K. (2004) Pyritization processes and greigite formation in the advancing sulfidization front in the Upper Pleistocene sediments of the Black Sea. *Geochim. Cosmochim. Acta* **68**, 2081–2093.

Niewöhner C., Hensen C., Kasten S., Zabel M. and Schulz H. (1998) Deep sulfate reduction completely mediated by anaerobic methane oxidation in sediments of the upwelling area off Namibia. *Geochim. Cosmochim. Acta* **62**, 455–464.

Oni O., Miyatake T., Kasten S., Richter-Heitmann T., Fischer D., Wagenknecht L., Kulkarni A., Blumers M., Shylin S. I., Ksenofontov V., Costa B. F. O., Klingelhöfer G. and Friedrich M. W. (2015) Distinct microbial populations are tightly linked to the profile of dissolved iron in the methanic sediments of the Helgoland mud area, North Sea. *Front. Microbiol.* **6**, 1–15.

Petzoldt L. R. (1983) Automatic selection of methods for solving stiff and nonstiff systems of ordinary differential equations. *SIAM J. Sci. Stat. Comput.* **4**, 136–148.

Postma D. and Jakobsen R. (1996) Redox zonation: Equilibrium constraints on the Fe(III)/SO4-reduction interface. *Geochim. Cosmochim. Acta* **60**, 3169–3175.

Poulton S. and Canfield D. (2005) Development of a sequential extraction procedure for iron: implications for iron partitioning in continentally derived particulates. *Chem. Geol.* **214**, 209–221.

Pyzik A. J. and Sommer S. E. (1981) Sedimentary iron monosulfides: kinetics and mechanism of formation. *Geochim. Cosmochim. Acta* **45**, 687–698.

Qu D., Ratering S. and Schnell S. (2004) Microbial reduction of weakly crystalline iron (III) oxides and suppression of methanogenesis in paddy soil. *Bull. Environ. Contam. Toxicol.* **72**, 1172–1181.

Rayleigh J. W. S. (1896) Theoretical considerations respecting the separation of gases by diffusion and similar processes. *Philos. Mag.*, 493–499.

Reeburgh W. (2007) Oceanic methane biogeochemistry. *Am. Chem. Soc.* **107**, 486–513.

Reed D. C., Gustafsson B. G. and Slomp C. P. (2016) Shelf-to-basin iron shuttling enhances vivianite formation in deep Baltic Sea sediments. *Earth Planet. Sci. Lett.* **434**, 241–251.

Reed D. C., Slomp C. P. and Gustafsson B. G. (2011a) Sedimentary phosphorus dynamics and the evolution of bottom-water hypoxia: A coupled benthic-pelagic model of a coastal system. *Limnol. Oceanogr.* **56**, 1075–1092.

Reed D. C., Slomp C. P. and de Lange G. J. (2011b) A quantitative reconstruction of organic matter and nutrient diagenesis in Mediterranean Sea sediments over the Holocene. *Geochim. Cosmochim. Acta* **75**, 5540–5558.

Reiche M., Torburg G. and Küsel K. (2008) Competition of Fe(III) reduction and methanogenesis in an acidic fen. *FEMS Microbiol. Ecol.* **65**, 88–101.

Rice A. L., Gotoh A. A., Ajie H. O. and Tyler S. C. (2001) High-precision continuous-flow measurement of δ13C and δD of atmospheric CH_4. *Anal. Chem.* **73**, 4104–4110.

Rickard D. and Luther, III, G. W. (1997) Kinetics of pyrite formation by the H2S oxidation of iron (II) monosulfide in aqueous solutions between 25 and 125°C: the mechanism. *Geochim. Cosmochim. Acta* **61**, 135–147.

Rickard D. and Luther, III, G. W. (2007) Chemistry of iron sulfides. *Chem. Rev.* **107**, 514–562.

Riedinger N., Formolo M. J., Lyons T. W., Henkel S., Beck A. and Kasten S. (2014) An inorganic geochemical argument for coupled anaerobic oxidation of methane and iron reduction in marine sediments. *Geobiology* **12**, 172–181.

Riedinger N., Kasten S., Gröger J., Franke C. and Pfeifer K. (2006) Active and buried authigenic barite fronts in sediments from the Eastern Cape Basin. *Earth Planet. Sci. Lett.* **241**, 876–887.

Riedinger N., Pfeifer K., Kasten S., Garming J. F. L., Vogt C. and Hensen C. (2005) Diagenetic alteration of magnetic signals by anaerobic oxidation of methane related to a change in sedimentation rate. *Geochim. Cosmochim. Acta* **69**, 4117–4126.

Rooze J., Egger M., Tsandev I. and Slomp C. P. (2016) Iron-dependent anaerobic oxidation of methane in coastal surface sediments: potential controls and impact. *Limnol. Oceanogr.* **61**, S267–S282.

Van Santvoort P. J. M., De Lange G. J., Thomson J., Colley S., Meysman F. J. R. and Slomp C. P. (2002) Oxidation and origin of organic matter in surficial Eastern Mediterranean hemipelagic sediments. *Aquat. Geochem.* **8**, 153–175.

Sapart C. J., van der Veen C., Vigano I., Brass M., van de Wal R. S. W., Bock M., Fischer H., Sowers T., Buizert C., Sperlich P., Blunier T., Behrens M., Schmitt J., Seth B. and Röckmann T.

() Simultaneous stable isotope analysis of methane and nitrous oxide on ice core samples. *Atmos. Meas. Tech.* **4**, 2607–2618.

Scheller S., Yu H., Chadwick G. L., McGlynn S. E. and Orphan V. J. (2016). Artificial electron acceptors decouple archaeal methane oxidation from sulfate reduction. Science 351(80-.), 703–707.

Schippers A. and Jørgensen B. B. (2002) Biogeochemistry of pyrite and iron sulfide oxidation in marine sediments. *Geochim. Cosmochim. Acta* **66**, 85–92.

Segarra K. E. A., Comerford C., Slaughter J. and Joye S. B. (2013) Impact of electron acceptor availability on the anaerobic oxidation of methane in coastal freshwater and brackish wetland sediments. *Geochim. Cosmochim. Acta* **115**, 15–30.

Seifert R., Nauhaus K., Blumenberg M., Krüger M. and Michaelis W. (2006) Methane dynamics in a microbial community of the Black Sea traced by stable carbon isotopes in vitro. *Org. Geochem.* **37**, 1411–1419.

Sivan O., Adler M., Pearson A., Gelman F., Bar-Or I., John S. G. and Eckert W. (2011) Geochemical evidence for iron-mediated anaerobic oxidation of methane. *Limnol. Oceanogr.* **56**, 1536–1544.

Sivan O., Antler G., Turchyn A. V., Marlow J. J. and Orphan V. J. (2014) Iron oxides stimulate sulfate-driven anaerobic methane oxidation in seeps. *Proc. Natl. Acad. Sci.* **111**, 4139–4147.

Sivan O., Shusta S. and Valentine D. L. (2016) Methanogens rapidly transition from methane production to iron reduction. *Geobiology* **14**, 190–203.

Slomp C. P., Mort H. P., Jilbert T., Reed D. C., Gustafsson B. G. and Wolthers M. (2013) Coupled dynamics of iron and phosphorus in sediments of an oligotrophic coastal basin and the impact of anaerobic oxidation of methane. *PLoS One* **8**, e62386.

Soetaert K. and Herman P. M. J. (2009) A Practical Guide to Ecological Modelling: Using R as a Simulation Platform. Springer.

Soetaert K. and Meysman F. (2012) Reactive transport in aquatic ecosystems: rapid model prototyping in the open source software R. *Environ. Model. Softw.* **32**, 49–60.

Soetaert K., Petzoldt T. and Meysman F. J. R. (2010) marelac: Tools for Aquatic Sciences. R Package Version 2.1.3.

Sohlenius G., Emeis K.-C., Andrén E., Andrén T. and Kohly A. (2001) Development of anoxia during the Holocene fresh-brackish water transition in the Baltic Sea. *Mar. Geol.* **177**, 221–242.

Torres M. E., Brumsack H. J., Bohrmann G. and Emeis K. C. (1996) Barite fronts in continental margin sediments: a new look at barium remobilization in the zone of sulfate reduction and formation of heavy barites in diagenetic fronts. *Chem. Geol.* **127**, 125–139.

Torres M. E., Mix A. C. and Rugh W. D. (2005) Precise δ13C analysis of dissolved inorganic carbon in natural waters using automated headspace sampling and continuous-flow mass spectrometry. *Limnol. Oceanogr. Meth.* **3**, 349–360.

Treude T., Krause S., Maltby J., Dale A. W., Coffin R. and Hamdan L. J. (2014) Sulfate reduction and methane oxidation activity below the sulfate-methane transition zone in Alaskan Beaufort Sea continental margin sediments: implications for deep sulfur cycling. *Geochim. Cosmochim. Acta* **144**, 217–237.

Vargas M., Kashefi K., Blunt-Harris E. L. and Lovley D. R. (1998) Microbial evidence for Fe(III) reduction on early Earth. *Nature* **395**, 65–67.

Wallace P. J., Dickens G. R., Paull C. K. and Ussler, III, W. (2000) Effects of core retrieval and degassing on the carbon isotope composition of methane in gas hydrate- and free gas-bearing sediments from the Blake Ridge. *Proc. Ocean Drill. Program. Sci. Results* **164**, 101–112.

Wang Y. and Van Cappellen P. (1996) A multicomponent reactive transport model of early diagenesis : Application to redox cycling in coastal marine sediments. *Geochim. Cosmochim. Acta* **60**, 2993–3014.

Wankel S. D., Adams M. M., Johnston D. T., Hansel C. M., Joye S. B. and Girguis P. R. (2012) Anaerobic methane oxidation in metalliferous hydrothermal sediments: influence on carbon flux and decoupling from sulfate reduction. *Environ. Microbiol.* **14**, 2726–2740.

Wegener G., Krukenberg V., Riedel D., Tegetmeyer H. E. and Boetius A. (2015) Intercellular wiring enables electron transfer between methanotrophic archaea and bacteria. *Nature* **526**, 587–590.

Westrich J. T. and Berner R. A. (1984) The role of sedimentary organic matter in bacterial sulfate reduction: The G model tested. *Limnol. Oceanogr.* **29**, 236–249.

Whiticar M. J. (1999) Carbon and hydrogen isotope systematics of bacterial formation and oxidation of methane. *Chem. Geol.* **161**, 291–314.

Xia X. and Tang Y. (2012) Isotope fractionation of methane during natural gas flow with coupled diffusion and adsorption/desorption. *Geochim. Cosmochim. Acta* **77**, 489–503.

Yoshinaga M. Y., Holler T., Goldhammer T., Wegener G., Pohlman J. W., Brunner B., Kuypers M. M. M., Hinrichs K. and Elvert M. (2014) Carbon isotope equilibration during sulphate-limited anaerobic oxidation of methane. *Nat. Geosci.* **7**, 190–194.

Zhou S., Xu J., Yang G. and Zhuang L. (2014) Methanogenesis affected by the co-occurrence of iron(III) oxides and humic substances. *FEMS Microbiol. Ecol.* **88**, 107–120.

Zhuang L., Xu J., Tang J. and Zhou S. (2015) Effect of ferrihydrite biomineralization on methanogenesis in an anaerobic incubation from paddy soil. *J. Geophys. Res. Biogeosci.* **120**, 876–886.

Zillén L., Conley D. J., Andrén T., Andrén E. and Björck S. (2008) Past occurrences of hypoxia in the Baltic Sea and the role of climate variability, environmental change and human impact. *Earth-Sci. Rev.* **91**, 77–92.

Associate Editor: Orit Sivan